

MDPI

Article

# Lodging Variability in Sorghum Stalks Is Dependent on the Biomechanical and Chemical Composition of the Stalk Rinds

Endalkachew Mengistie <sup>1</sup>, Norbert Bokros <sup>2</sup>, Seth DeBolt <sup>2</sup> and Armando G. McDonald <sup>1,\*</sup>

- Forest and Sustainable Products Program, College of Natural Resources, University of Idaho, Moscow, ID 83844, USA
- Plant Physiology, Department of Horticulture, Agricultural Science Center North, University of Kentucky, Lexington, KY 40546, USA
- \* Correspondence: armandm@uidaho.edu; Tel.: +1-208-885-9454

Abstract: Stalk lodging contributes to significant crop yield losses. Therefore, understanding the biomechanical strength and structural rigidity of grain stalks can contribute to improving stalk lodging resistance in crops. From the structural constituents of the stalk, the rind provides the principal structure, supporting cells against tension and bending loads. In this work, the biomechanical and viscoelastic behavior of the rind from the internodes of two sweet sorghum varieties (Della and REDforGREEN (RG)), grown in two different growing seasons, were evaluated by three-point microbending tests using a dynamic mechanical analyzer (DMA). In addition, the chemical composition of rinds and the microfibril angle (MFA) of the cell wall were determined using XRD. The results revealed that the biomechanical behavior of Della varieties was stiffer and more resistant to loads than that of RG varieties. Two features of the rind biomechanical properties, flexural modulus (FM) and flexural strength (FS), showed a significant reduction for RG. Particularly, a reduction in FS of 16-37% and in FM of 22-41% were detected for RG1. Changes in the stalks' rind biomechanical properties were attributed to cell wall components. Total lignin and glucan/cellulose contents were positively correlated with the FM and FS of the rind. Subsequently, an increase in the two cell wall components drove an increase in stiffness. Furthermore, the MFA of the rind was also found to influence the rind strength.

**Keywords:** biomechanical properties; dynamic mechanical analysis; three-point bending; compositional analysis; viscoelastic properties; microfibril angle



Citation: Mengistie, E.; Bokros, N.; DeBolt, S.; McDonald, A.G. Lodging Variability in Sorghum Stalks Is Dependent on the Biomechanical and Chemical Composition of the Stalk Rinds. *Crops* **2024**, *4*, 3–26. https:// doi.org/10.3390/crops4010002

Received: 25 October 2023 Revised: 26 December 2023 Accepted: 5 January 2024 Published: 11 January 2024



Copyright: © 2024 by the authors. Licensee MDPI, Basel, Switzerland. This article is an open access article distributed under the terms and conditions of the Creative Commons Attribution (CC BY) license (https://creativecommons.org/licenses/by/4.0/).

## 1. Introduction

Crops are widely grown across the globe, mainly for food, and crop yield can be reduced significantly by lodging. Lodging is defined as an irreversible structural failure of the stem both at the microstructure and at the macrostructure level before harvesting [1]. Lodging induces the dislocation of stalks from their vertical position, subsequently leading to a breakage of the stalk on the ground [2]. Lodging limits grain yield in cereal crops such as sorghum, maize, rice, and wheat [3]. Particularly in high-yielding cereal crops, lodging may result in global annual yield reductions of 2-30% [4], depending on the stage of growth. The biomechanical properties of stalks are important in determining their strength, which in turn impacts resistance against lodging. Therefore, enhancing the biomechanical strength of the stem is essential for lodging resistance and increasing annual yield. Despite its enormous economic impact on commercial crops, the stem lodging mechanism is not clearly understood. Previous studies used methods such as bending tests, histochemical methods, rind penetrometers, and crushing strength measurements to understand stem biomechanical behavior [5]. However, these approaches are inadequate to fully understand the buckling of stem structures, as the chemical composition of the stalks are not considered. Thus, approaches involving chemical analysis together with an analysis

of the biomechanical behavior of the crops will improve our understanding in order to develop lodging-resistant varieties, enhancing agricultural productivity and narrowing the knowledge gap in stalk lodging mechanisms.

The degree of lodging depends on many plant characteristics and other environmental aspects. Plant characteristics regulate their height and architecture and thus contribute to lodging resistance [4]. Plants have adapted unique stem anatomical, morphological, and hierarchical architectures to maintain structural integrity when subjected to loads [6,7]. The anatomical (e.g., vascular bundles, parenchyma and sclerenchyma cells), morphological (e.g., plant height, internode length, stem diameter, rind thickness), biochemical (e.g., structural and nonstructural polymer composition), and genetic traits of the stalk contribute to lodging susceptibility [8–10]. The anatomical features of stems such as sclerenchyma tissue can impact lodging resistance. Cultivars with thicker sclerenchyma tissue with high a content of cellulose and lignin scored lower lodging rates than cultivars with thin-layered mechanical tissues [11]. The biochemical traits of stems, such as lignin, cellulose, and hemicellulose, play a major role in biomechanical strength and rigidity. Lignin is a dominant structural component of secondary cell walls and middle lamella that provides strength to plants and to the rigidity of basal stems [12,13]. Higher lignin and cellulose contents in crop stems result in the higher rigidity of the culm [14], enhanced lodging resistance, and enhanced stem strength [15]. Cellulose contributes to the tensile strength of cells and stems, while lignin provides stiffness. In addition, nutrients like silicon play a vital role for the growth and development of cell walls and are associated with improving the biomechanics of plants and resistance to lodging, drought, UV radiation, and pathogens [16].

Sorghum stalks fail structurally because of their weak biomechanical properties [17]. The biomechanical properties of sorghum internodes were found to exhibit significantly lower flexural modulus (FM), flexural strength (FS), and flexural rigidity than the nodes. Moreover, nodes of sorghum were two- to three-fold stronger, stiffer, and more rigid than the internodes, and were less liable to the structural failure of the stalk [18]. Plant cell walls are microfibril-based nanocomposites with a distinct polymer matrix arrangement and structure. The higher-order organization of cellulose microfibrils into bundles and discrete lamellae results in different rheological and biomechanical properties [19]. Therefore, an investigation of stalk failure, beyond simply determining the elastic modulus and ultimate strength [17], needs to be correlated with the structural compositions of the cell wall for a better understanding of sorghum biomechanical and lodging behavior.

Stems provide physical support to the leaves and grain and aid the transport of water and nutrients in crops [20]. Sorghum stems have sclerenchyma (epidermis and rind with many sub-epidermal cell layers) as well as parenchyma tissue (pith, consisting of vascular bundles and soft tissues) [17]. Because parenchyma cells can absorb the effects of environmental forces such as light, wind, and rain without mechanical damage, stem standability increases with parenchyma layer thickness [12]. Although pith parenchyma cells play a vital role in stabilizing the stem and reducing the risk of local buckling and collapse, up to 80% of the mechanical strength of a stalk comes from the rind [10,21]. Thus, the mechanical strength of stalks primarily depends on the rind of the internode. The rind is a dense and fibrous tissue with higher mechanical strength, providing the principal structure supporting cells against tension and bending loads [14]. Studies based on the dissection of stalk strength into its constituent features showed that the structural composition of the rind, not the pith or total girth, appears to be the most important stalk strength determining component [22]. Cell wall chemical composition studies on corn stalk showed that the rind had higher lignin and cellulose content than other components [22]. Therefore, it is necessary to evaluate the biomechanical and viscoelastic nature of sorghum rinds to reveal the macromolecular and lodging variation of stems.

Plant cell wall layers are considered a nanofiber-reinforced composite material consisting of helically wound crystalline cellulose microfibrils embedded in a matrix of amorphous cellulose, hemicelluloses, and lignin [23]. Dynamic mechanical analysis (DMA) can be used to examine composite properties and the response of individual cell wall components in

situ and enlightens the individual cell wall polymers' contributions as well as their interactions [24]. DMA has been applied to investigate the viscoelastic and mechanical properties of barley stems [25]. The present study aims to evaluate the rind biomechanical strength from two sorghum stalk varieties using DMA and correlate it with the accumulation of the main polymeric components of the cell wall (cellulose, hemicellulose, and lignin).

#### 2. Results and Discussion

## 2.1. Micro-Biomechanical Bending Tests

A bending test is a common mechanical phenotyping method to evaluate stalk strength and lodging, which can induce a similar failure pattern to that observed in naturally lodged crops [26]. Stalk strength and stiffness are greatly influenced by its geometry (e.g., diameter and rind thickness). The rind constitutes up to 80% of the material strength of a stalk [21]. Thus, bending tests were performed on the rind to determine the FS and FM of the internodes (Figure 1a) from their stress–strain curves (Figure 1b). The FS describes the stress required to cause a rind to fail and can be taken as the ultimate resistance when the rind is exposed to bending stress [27], whereas the rind's stiffness is measured by the FM. Both FM and FS are the main indicators of the lodging resistance of crop stalks [28].

The FM of the rinds was shown to decrease from the bottom IN1 towards the top section (IN5) of the stem, which reveals the variation in physico-mechanical properties along the internodes (Figure 1c). The same trend (a decrease in FM with IN height) have been reported in maize [29] and rice stems [30]. The axial FM variation could be associated with the morphological, anatomical, and compositional heterogeneity of the internodes [31]. The bottom basal internodes (IN1-IN2) were stiffer than the upper internodes (IN3-IN5), except for RG1 where IN2 and IN3 were similar (Figure 2c). The average FM values (Figure 1d) along the internodes for D1, RG1, D2, and RG2 were 2.1, 1.4, 2.7, and 2.3 GPa, respectively. These FM results reveal that both RG1 and RG2 were significantly lower than D1 and D2. The variations in FM for RG were likely from differences in their composition compared to the Della variety (discussed later). Differences between the two growing seasons were observed. This observation reflects the pronounced impact of seasonal and environmental conditions on properties. Stem biomechanical property variations among different sorghum genotypes in terms of stem strength, rigidity, and stiffness have been reported [32]. Furthermore, Wright et al. [33] had shown for barley that the biomechanical properties of wild-types were stiffer than their mutant varieties. In addition, the FM for wheat was 1.1-2.2 GPa, and for barley it was 1.1-1.3 GPa. Similar to fiber-reinforced composites, stem structures exhibit anisotropy (aligned fibers) in terms of morphology, structure, stress distribution, growth, and development [14], which might lead to heterogeneity in the axial FM. This indicates that FM predicted 81% of the variation in maize stalk strength and the predominant parameter in predicting maize stalk lodging [34]. Thus, considering the FM variations, Della could be regarded as a mechanically strong variant than the RG mutant within each growing season.

The FS of the D1, RG1, D2, and RG2 internode rinds ranged from 49.2–63.9, 30.9–58.1, 58.2–72.0 and 46.7–69.7 MPa, respectively (Figure 1e). Along the internodes, the results demonstrate (Figure 1e) a decrease in FS from the basal internode upwards, and this trend has been previously reported [18]. Moreover, Zhang et al. [35] demonstrated for maize stalk rinds that the lower internodes had higher FS than the upper internodes. Researchers have shown that stalk lodging occurred in the upper basal internodes [36]. Across the varieties, the FS of Della was found to be significantly higher than its corresponding RG (p < 0.001) at all internodes, indicating its biomechanical property variation. On an average basis (Figure 1f), the FS of D2 and D1 rinds were about 8.2% and 27% higher, respectively, than RG2 and RG1. These results suggest that the FS of RG1 was considerably reduced, which could be a combined effect of mutation and the growing season. Moreover, it can also be explained by a significant reduction in lignin and glucan/cellulose content in RG1 (discussed later). Across the growing seasons, D1 and RG1 were 15–18% and 25–70% weaker, respectively, than D2 and RG2. Stalk lodging was found to be closely

associated with bending strength [37]; thus, according to the FS values of stalk rinds, the RG variety could be structurally more lodging-susceptible. Sorghum rind thickness and strength were found to be highly correlated with lodging [38], which supports the lodging susceptibility of RG. Sclerenchyma cells around the vascular bundles of the stem are responsible for mechanical strength; thus, a reduction in the flexural properties of RG could be related to reductions in lignin and carbohydrate accumulations in sclerenchyma cells, inducing stem lodging [10].

## 2.2. Viscoelastic Properties

The viscoelastic properties of both Della (control group) and RG IN1 rinds were evaluated in terms of flexural storage modulus (E'), loss modulus (E''), and dampening factor (tan  $\delta$ ) as a function of relative humidity (RH). E' represents part of the deformation that can be recovered, thus characterizing the elastic component of a material, whereas E''reflects the proportion of the deformation that cannot be recovered which is dissipated as heat due to viscous flow in a material [39]. The E' and E" curves (Figure Figure 2a and Figure 2b, respectively) represent typical characteristics of wood's viscoelastic behavior [40]. The E' values of Della were higher than those of the RG varieties, with D2 having the highest value of 3.6 GPa at 0% RH. The decreasing order of E' was D2 > RG2 > D1 > RG1. Generally, E' decreases with an increase in RH (Figure 2a) due to the plasticizing effect of water [40]. As RH increases, moisture diffusion gradients are developed at the surface towards the center of the sample. Consequently, water can plasticize the cell wall matrix and decrease the rind E' [41]. A reduction in E' of 11%, 9%, 14%, and 12% was observed going from 0 to 80% RH for D2, RG2, D1, and RG1 samples, respectively. The water diffusion rate into the cell walls will depend on the stalk's structure and composition [42]. The viscoelastic behavior of the stalk rind will also be influenced by the hydroxyl groups (and other polar groups) present in amorphous zones of cellulose, hemicellulose, and lignin that interact with water [43]. Consequently, hydrogen bonds in the amorphous regions will be disrupted, and new hydrogen bonds between water molecules and hydroxyl groups will be formed. The hydration of the cell wall polymers leads to the expansion and swelling of the cell wall microstructures, which in turn results in a variation and decrease in E' [44]. The extent of change of E' was limited because of the low MC of the samples.

As RH/moisture continues to increase, more energy is dissipated, and E" increases (Figure 2b). D2 showed the highest E" (177 MPa at 0%RH) compared to RG2; however, D1 was slightly greater than RG1 (lowest at 85 MPa at 0% RH). An increase in E" was an indicator of enhanced plasticization [45]. Tan  $\delta$  represents the damping or inner friction of a viscoelastic system. For the stalk rind, tan  $\delta$  increased with RH, which demonstrated that the absorbed water acted to increase energy dissipation (Figure 2c). Similar results have been reported in wood [46]. Going from 0 to 80% RH, tan  $\delta$  was shown to increase by 114–120% for the stalk rind. The D2 samples have a higher tan  $\delta$  compared to the other samples, indicating high non-elastic deformation. On the other hand, D1 and RG2 had relatively lower tan  $\delta$ , showing more elastic behavior. The clear variation in E" and tan  $\delta$  among varieties is shown in separate plots in supplementary material Figure S1a,b.

In addition to moisture, viscoelastic properties of lignocellulosic materials are also influenced by temperature and were measured [25]. E' was shown to decrease with increasing temperature up to ~70 °C and then started to increase to a peak maximum at about 88 °C (Figure 3a). Unlike polymers, the dynamic behavior of wood materials with temperature variation was not straightforward due to the coupling of thermal properties of three cell wall constituent polymers [47]. This peak at about 88 °C could possibly be due to the aggregation and reformation of a network structure of lignin cross-linking at ~85 °C [48] and/or lignin relaxation [49]. Similar trends have been reported in polymers associated with cold crystallization [50]. The E' values for the various stalk rinds were significantly different and decreased in the order D2 > RG2 > D1 > RG1, which was related to lignin content (discussed later). These results agree with previous findings in transgenic aspen [51].

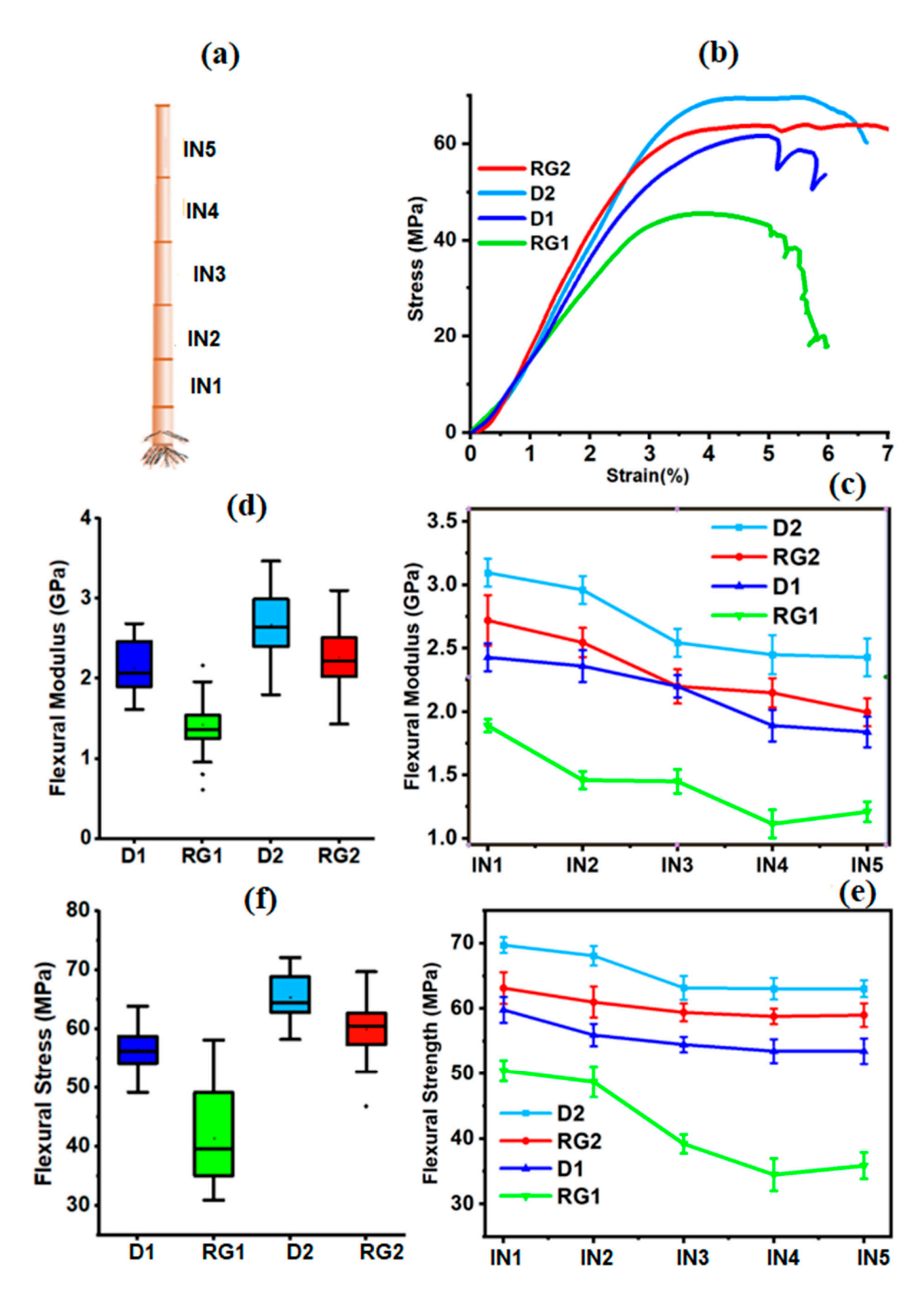


**Figure 1.** (a) Schematics of stalks from internodes (IN1-IN5); (b) representative flexural stress–strain curves of Della1 (D1), Della2 (D2), RG1, and RG2 stalk rinds; (c) flexural modulus (FM) measured at various internodes (IN); (d) box plots of averaged FM values for sorghum stalk rinds over IN1-IN5; (e) flexural strength (FS) along the internodes (IN1-IN5); and (f) box plots of averaged FS for D1, RG1, D2, and RG2.

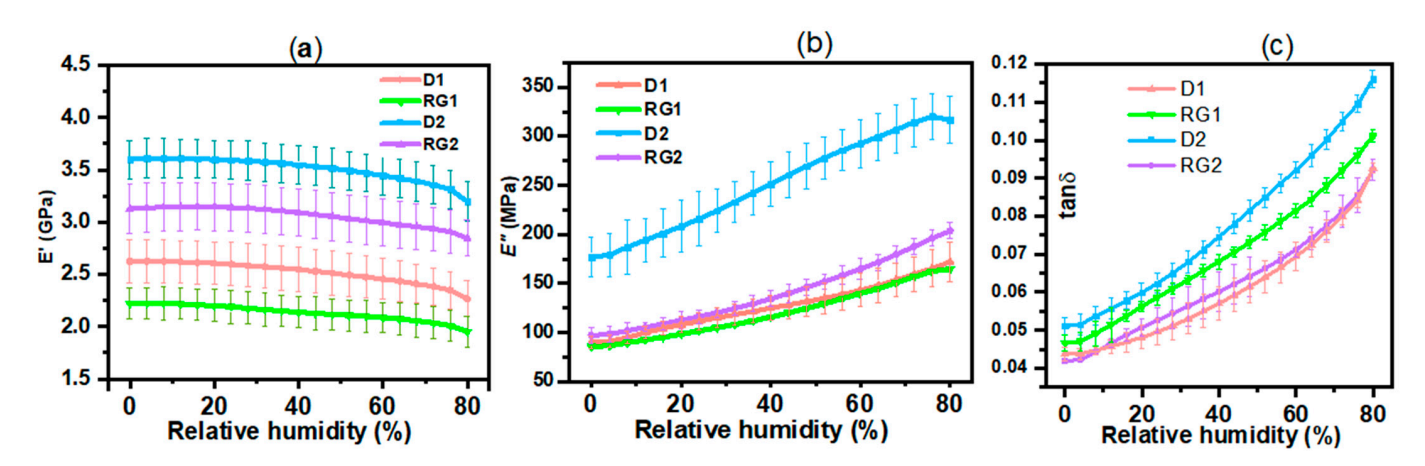


**Figure 2.** (a) Storage modulus (E'); (b) loss modulus (E"); and (c) damping factor (tan  $\delta$ ) as a function of relative humidity (RH) for sorghum stalk IN1 rind from Della and RG varieties (whiskers represent the standard error mean).

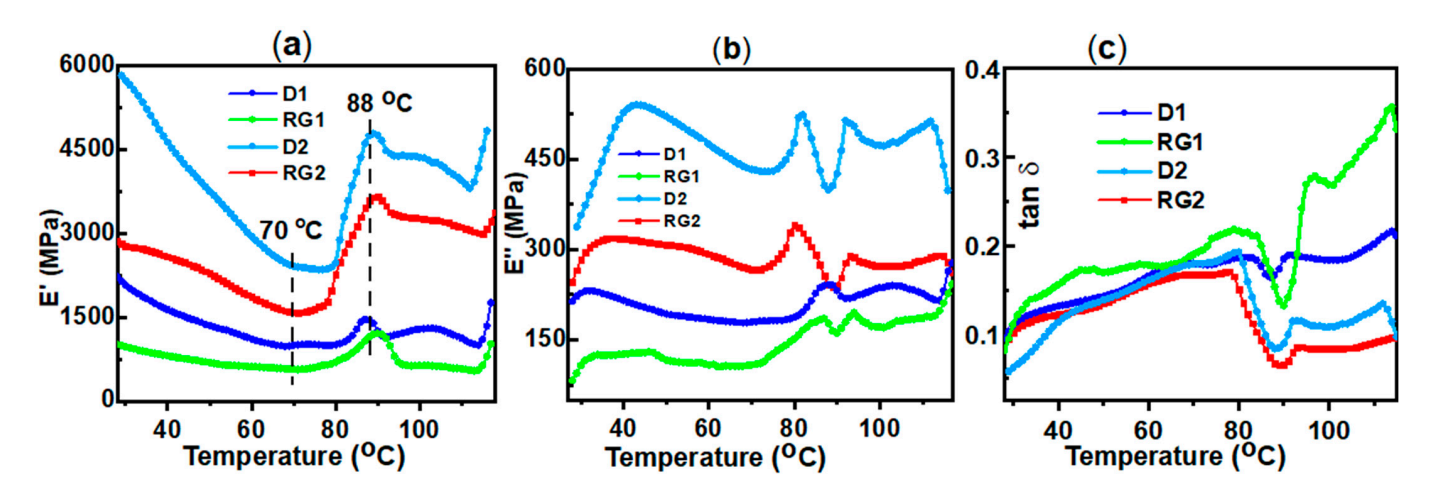


**Figure 3.** (a) Storage modulus (E'); (b) loss modulus (E"); and (c) tan  $\delta$  thermograms of sorghum in 1 rind at IN3 for D1, RG1, D2, and RG2 samples.

The in situ glass transition temperature  $(T_g)$  of lignin in the stalk was determined from the peaks of E'' and  $\tan \delta$  [51,52] (Figure 3b,c and Table 1). In situ  $T_g$  values were consistent with the literature for wood [48]. Two distinct glass transitions  $(T_{g1}$  and  $T_{g2})$  were observed in the rind samples (Figure 3b). For D2,  $T_{g1}$  was at 82 °C and  $T_{g2}$  at 92 °C, whereas for RG1,  $T_{g1}$  was at 80 °C and  $T_{g2}$  at 93 °C. For the D1 sample, only one  $T_g$  peak at 98 °C was observed (Table 1). Two minor peaks/shoulders at 87 °C and 94 °C were detected for RG1. Two-phase thermal transitions have been observed in wheat straw and spruce wood, in which  $\alpha$ -transitions ( $\alpha$ 1) of 53 °C (straw) and 91 °C (spruce) associated with lignin was reported [51]. The observations of two transition peaks could be related to the less-rigid and more-rigid phases of lignin, which are interwoven with amorphous and crystalline cellulose, respectively [53]. Furthermore, this can also reflect the supramolecular heterogeneity in the rind and in situ thermo-rheological complexity of lignocellulosic substrate [54]. The different thermo-rheological results revealed that lignin content plays a role in structural variation within the varieties [51]. The  $T_g$  of lignin was shown to be dependent on moisture content [55]. Values for  $T_g$  of 72–88 °C for transgenic aspen lignin [51] and 80–95 °C for other woods [48,56] have been reported.

93

94

E''tanδ  $tan\delta_{maximum}$ Sample  $T_{g1}$  (°C)  $T_{g1}$  (°C) T<sub>g2</sub> (°C)  $T_{g2}$  (°C)  $tan\delta_{max1}$ tan8max2 82 92 80 92 0.115 D2 0.192

78

83

79

93

91

97

0.170

0.186

0.218

0.086

0.188

0.280

Table 1. Glass transition temperatures (Tg) of stalk IN1 rind from D2, RG2, D1, and RG1 at IN3 determined by DMA.

The results also revealed that the first transition  $T_{g1}$  from the tan  $\delta$  peak slightly shifted towards lower temperatures as compared to  $T_{\rm g1}$  from  $E^{\prime\prime}$  (Table 1). On the other hand,  $T_{g2}$  determined from E'' and  $tan \delta$  were only slightly different. The  $tan \delta$  maximum at the distinct peak ( $tan\delta_{max}$ ), which roughly reflects the quantity of the relaxing polymer [46], were different: (RG1 > D2 > D1 > RG2) at  $\tan \delta_{max1}$  and (RG1 > D1 > D2 > RG2) at  $\tan \delta_{max2}$ (Table 1). Given that there was a significant difference in lignin content and composition (discussed later) between the samples, the variation in  $\tan \delta_{max}$  between the varieties was expected. However, the correlation of lignin content and syringyl/guaiacyl (S/G ratio) with in situ T<sub>g</sub> demonstrated that T<sub>g</sub> was not significantly affected by either lignin content or composition. Unlike extracted lignin, the in situ T<sub>g</sub> might be highly impacted by molecular architecture and lignin–carbohydrate complex in the cell wall [57].

#### 2.3. Stress Relaxation in Stalk Rind

80

88

87

RG2

D1

RG1

Plant cell wall structural components (cellulose, lignin, and hemicellulose) behave as an anisotropic composite material [58]. As polymers, cell wall components exhibit timedependent mechanical behavior, indicating the viscoelastic nature of plant material [59]. The viscoelastic nature of plant cell walls can be described by mechanical models consisting of both pure elastic springs and ideal viscous dashpots [60] and developed based on rheological principles [61]. The generalized Maxwell model (GMM) was applied to fit the stress relaxation of sorghum rind according to Equation (1) for (n = 3). The experimental and fitted modulus of relaxation for D1, D2, RG1, and RG2 is shown in Figure 4a, and the model parameters, equilibrium modulus of relaxation  $(E_{\infty})$ , and coefficients  $(E_1-E_3)$  are summarized in Table 2. The findings revealed that when the rind was exposed to constant strain and maintained over time, the internal stress developed decayed exponentially from their initial maximum to an ultimate equilibrium state. Two distinct relaxation stages (region i and ii, Figure 4a) were observed. Initially (t < 2 min, i), the modulus decreased exponentially due to a high rate of relaxation just after the application of maximum load, after which the curve flattened (t > 2 min, ii) and approached an equilibrium. Previous the studies on viscoelastic properties of barley stems reported two-stages of relaxation [25]. The elastic deformation was due to the distortion/breaking of bonds such as hydrogen bonds, van der Waals interactions, and electrostatic forces, which provide adhesion between the cellulose and hemicellulose–lignin matrix and are likely responsible for the rapid relaxation [62]. The cellulose and hemicellulose-lignin matrix will become more mobile, and the loading stress will be released as these weak bonds break. On the other hand, the slow relaxation stage may be attributed to conformational changes and strong covalent bonds. Significant variations in stress relaxation between rinds were observed (Figure 4a). This variation in stress relaxation behavior was consistent with the determined relaxation modulus from the GMM, shown by their equilibrium modulus ( $E_{\infty}$ ) in Table 2. The modulus of relaxation (Table 2) of the Della varieties was significantly higher than their corresponding RG varieties. D2 had the highest  $E_{\infty}$  of 2231 MPa, followed by RG2 (1368 MPa), D1 (1180 MPa), and RG1 (923 MPa). The model parameters  $(E_1-E_3)$  contribute to the initial modulus  $(E_0)$ , of which the samples had the following order: D2 > RG2 > D1 > RG1 (Table 2 and Figure 4a). On the other hand, the relaxation times  $(\tau_1 - \tau_3)$  determine the rate of change of the  $E_{\infty}$ .

The larger the relaxation time, the smaller the rate of change of  $E_{\infty}$ , and vice versa. In this regard, D2 had significantly higher relaxation times  $(\tau_1 - \tau_3)$  than the other samples. The stress relaxation behavior of lignocellulosic material can significantly vary and was influenced by factors such as genetics and cell wall composition, as seen in wheat straw cultivars [60]. The extent of stress relaxation and the rate at which it occurs is a critical factor in determining the effectiveness and performance of materials.

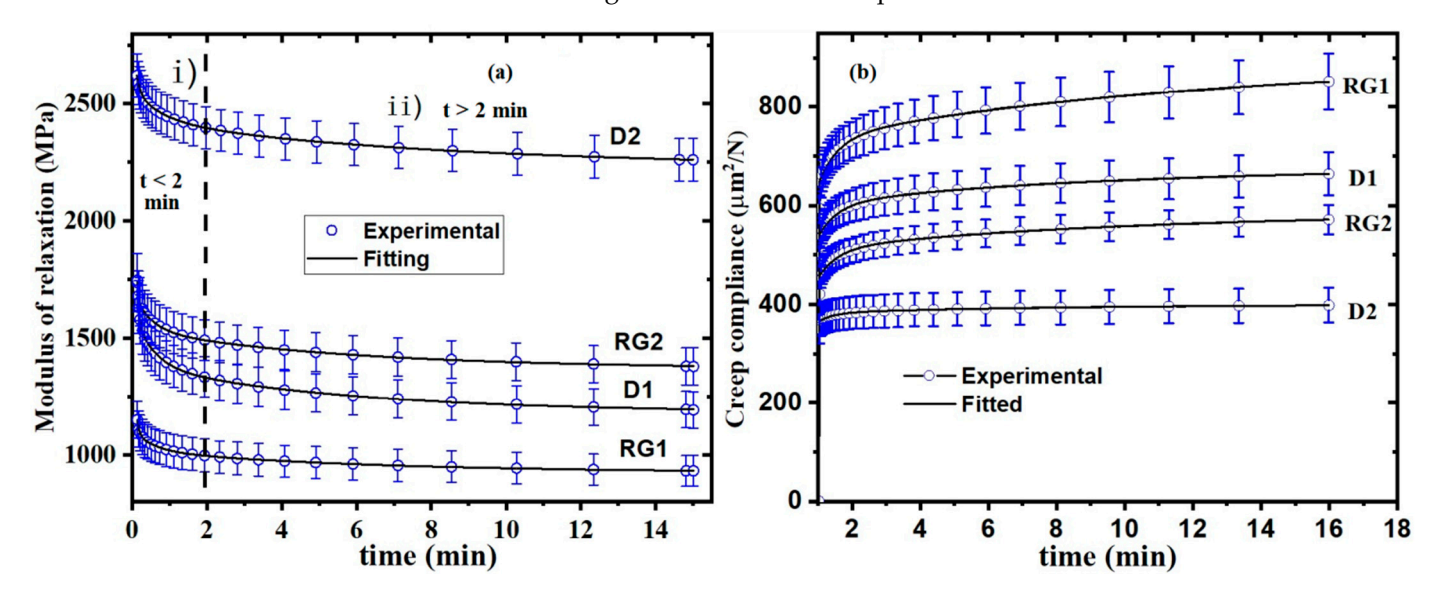


**Figure 4.** (a) Experimental and fitted modulus of relaxation; and (b) creep behavior for stalk IN1 rinds of Della1 (D1), Della2 (D2), RG1, and RG2 samples. Whiskers represent the standard error mean, and each point represents the average value of several measurements.

**Table 2.** Stress relaxation generalized Maxwell model parameters for D1, RG1, D2, and RG2 sorghum IN1 rinds.

Sample	$E_{\infty}$ (MPa)	E <sub>1</sub> (MPa)	$\tau_1$ (min)	E <sub>2</sub> (MPa)	τ <sub>2</sub> (min)	E <sub>3</sub> (MPa)	τ <sub>3</sub> (min)	E <sub>0</sub> (MPa)	$R^2$
D1	$1180\pm21$	$421\pm57$	$0.054 \pm 0.003$	$205.1\pm2.1$	$0.52 \pm 0.04$	$206.7 \pm 4.7$	$5.6 \pm 0.4$	$2013 \pm 15$	99.96
RG1	$923 \pm 19$	$225\pm12$	$0.054\pm0.004$	$91.8 \pm 3.9$	$0.52\pm0.04$	$96.5 \pm 1.7$	$6.2 \pm 0.4$	$1336\pm16$	99.96
D2	$2231 \pm 66$	$291\pm16$	$0.103 \pm 0.006$	$133.2\pm4.2$	$0.76 \pm 0.06$	$198.7 \pm 2.4$	$7.9 \pm 0.5$	$2854 \pm 9$	99.98
RG2	$1368\pm14$	$567\pm25$	$0.033 \pm 0.004$	$168.6 \pm 7.7$	$0.46\pm0.04$	$168.4\pm3.6$	$5.7 \pm 0.4$	$2271\pm20$	99.93

#### 2.4. Creep Behavior of Rinds

Creep compliance measures continuous deformation under constant stress over time [63]. The creep behavior of the rind was evaluated; experimental and fitted creep compliance is shown in Figure 4b, and model parameters determined based on Equation (2) are summarized in Table 3. The creep behavior of the IN1 rinds (Figure 4b) showed instantaneous deformation, the elastic response, and viscous deformation, as verified by the literature [64]. The results (Figure 4b) revealed that the Della variety had significantly lower initial creep compliance ( $C_0$ ) than its corresponding RG, which indicates an increase in deformation resistance. Initially upon loading, the material had C<sub>0</sub> due to an instantaneous elastic deformation corresponding to bond distortion [65]. It is shown (Table 3) that the  $C_0$  of samples were significantly different and ranked in the following order: RG1 (372  $\mu$ m<sup>2</sup>/N) > D1 (356  $\mu$ m<sup>2</sup>/N) > RG2 (307  $\mu$ m<sup>2</sup>/N) > D2 (295  $\mu$ m<sup>2</sup>/N). The higher C<sub>0</sub> shows higher elastic deformation due to bond distortion, and therefore RG1 showed the highest rate of deformation and was proven to have the lowest biomechanical strength (FM and FS). A larger instantaneous deformation in RG1 implies that biopolymers respond to the stress and orient along the stress direction in a short period, and the subsequent applied stress makes the additional orientation and rearrangement of chains impossible [66], which results in greater deformation. The results were consistent with bending strength and stress

relaxation behavior, which both showed the higher deformation resistance of D2. Higher creep is associated with poor performance by the polymeric building blocks of the plant cell wall's materials [14]. This suggests that the cell structure of Della was more resistant than that of RG, consequently enhancing the micromechanics of the cell wall that ultimately leads to improved macro-mechanical properties. Polymers with higher crystallinity, larger side groups, and higher molecular weight exhibit reduced polymer chain mobility, and consequently they have higher resistance to creep and stress relaxation [67]. The  $C_0$  of the varieties was found to be inversely proportional to lignin content.

Table 3. Creen	compliance mo	del parameters	for D1, R	G1, D2,	, and RG2 sorghum rinds.
----------------	---------------	----------------	-----------	---------	--------------------------

Sample	$C_0 (\mu m^2/N)$	$C_1 (\mu m^2/N)$	τ <sub>1</sub> (min)	$C_2 (\mu m^2/N)$	τ <sub>2</sub> (min)	$R^2$
D1	$356 \pm 9$	$80.2\pm2.3$	$8.9 \pm 0.0$	$240\pm1$	$0.7 \pm 0.0$	99.96
RG1	$372 \pm 10$	$170 \pm 6$	$11.9\pm0.0$	$353 \pm 2$	$0.69 \pm 0.0$	99.97
D2	$296 \pm 8$	$74.7 \pm 1.2$	$0.61 \pm 0.4$	$19.3 \pm 1.2$	$7.9 \pm 0.02$	99.97
RG2	$307 \pm 5$	$210 \pm 5$	$0.7 \pm 0.0$	$80.5 \pm 0.4$	$9.6 \pm 0.5$	99.98

The other model parameters ( $C_1$  and  $C_2$ ) contribute to long-term compliance, corresponding to the rubbery extension of the material [68], and the retardation times ( $\tau_1$  and  $\tau_2$ ) showed the times required to change the compliance of each series in the model. Even though creep and relaxation were both manifestations of the same molecular mechanisms and were related, converting one into the other was not attempted. This was mainly because of different experimental conditions and the need for long times for the attainment of equilibrium, without which the model could result in an overestimated parameter.

#### 2.5. Compositional Analysis

## 2.5.1. FTIR Spectral Analysis

FTIR spectroscopy was performed to determine the chemical features of the IN1 rind samples (Figure 5). Band assignments are given in Supplementary Table S1. Although the average spectral trends were similar, distinct absorption bands for RG1 were detected (Figure 5), which was likely related to cell wall compositional variability. A strong absorption band at 1030 cm<sup>-1</sup> appeared from C–O–C glycosidic linkage [69]. Typical S and G lignin bands were observed at 1320 and 1230 cm<sup>-1</sup>, respectively [70]. A lower spectral absorption intensity of RG1 relative to D1, D2, and RG2 was found (Figure 5), most likely associated with its reduced glucan and lignin contents (discussed later). A characteristic absorption band at 1370 cm<sup>-1</sup> due to C–H bending from cellulose and hemicelluloses was also detected. A band intensity variation at 1605 cm<sup>-1</sup>, attributed to skeletal C=C vibrations in S and G lignin coupled with C=O stretching, was also observed (Figure 5), revealing the lignin content variation between samples [71].

# 2.5.2. Crystallinity and MFA Analysis

Cellulose crystallinity (CI) in the fibrovascular bundles for the sorghum IN1 rinds was evaluated by XRD on powdered samples (Supplementary Figure S1 and Table 4). The XRD diffractograms confirms the presence of cellulose I crystals with peaks at  $2\theta$  of  $15.5^{\circ}$  and  $21.9^{\circ}$ , which are respectively assigned to [(1–10) and (110) overlapped] and (200) lattice indices [72]. XRD peak indexing was determined based on the crystalline structure of cellulose I $\beta$ . The deconvolution of the diffractogram (Supplementary Figure S2) revealed a broad amorphous structure centered at  $2\theta$  of  $18.5^{\circ}$  [73,74]. The CI of D2 was significantly higher than all samples. However, there was no difference between RG1 and D1, while RG2 was considerably more crystalline than D1 and RG1 (Table 4). The CI trend was consistent with reported values [75] and varied among varieties [76]. Sorghum stems have been reported to have CI of 39% [77]. The crystallinity of cellulose in D2 was 13.1% higher than RG2. The relatively higher crystallinity of D2 might contribute to its biomechanical stiffness. Regardless of season and variety, the grain size of cellulose I in all varieties was not significantly different. The effect of crystallite size on the intensity of amorphous

and crystallinity index was demonstrated by French and Santiago Cintrón [78]. The CI calculation considers both (200) and (110) peaks with respect to total area including larger amorphous regions.

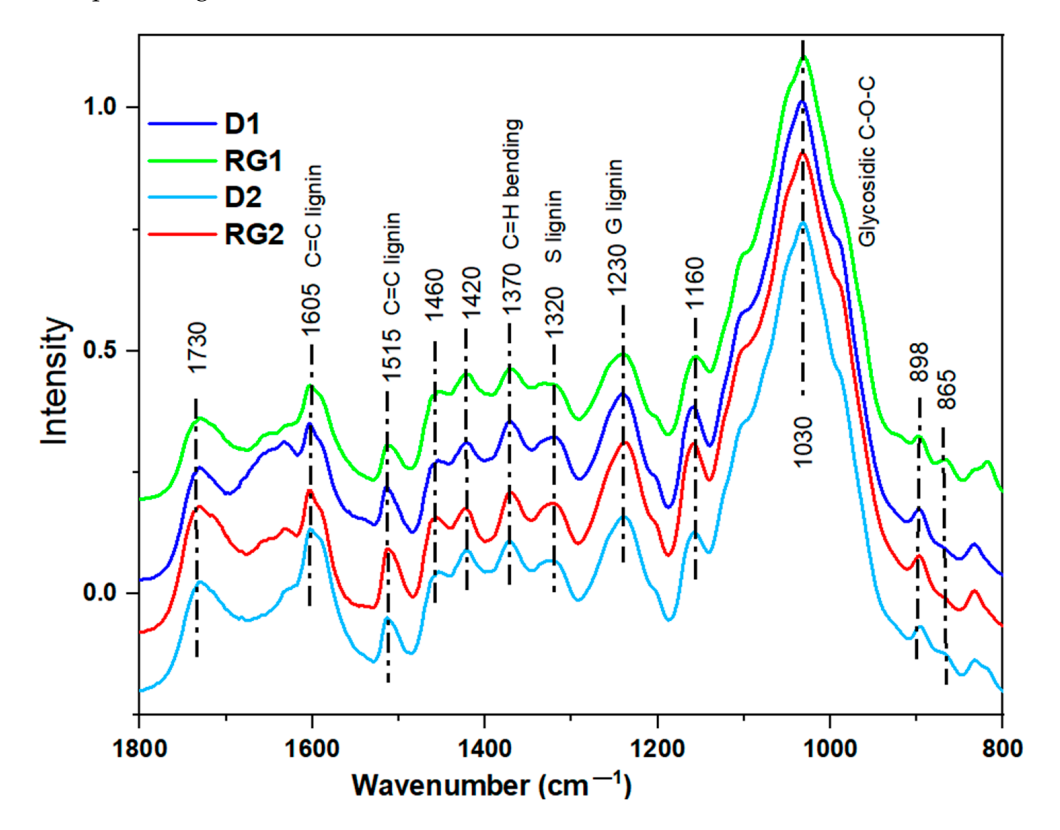


Figure 5. FTIR spectra of sorghum rinds from D1, RG1, D2, and RG2 varieties in the fingerprint region.

**Table 4.** Crystallinity index (CI) (with standard error mean) and grain size (L) of cellulose in sorghum stalk rinds.

Sample	CI (%)	L (nm)
D2	$43.2\pm0.4$	$3.1\pm0.2$
RG2	$38.2 \pm 0.5$	$3.2\pm0.1$
D1	$36.6 \pm 0.4$	$3.3 \pm 0.1$
RG1	$36.6\pm0.2$	$3.1 \pm 0.3$

The ultrastructure of the cell walls of wood and grasses such as bamboo has been found to be different [79], with some having thick-walled fibers with a polylamellate structure. Cellulose microfibril angle (MFA) in the fibrovascular bundles, deviation in their orientation from the fiber axis, highly affects the biomechanical properties of fibers and stalks. Thus, an estimated MFA of the IN1 rinds, based on the protocols of de Souza et al. [80], was investigated to evaluate their orientation, which plays the most important role in their mechanical properties. The X-ray diffraction pattern of an intact rind sample is shown in Figure 6a (and Supplementary Figure S2). It was found that the mean MFA of rinds (Figure 6b) decreased in the order of RG1 (30.6°  $\pm$  0.9) > D1 (27.0°  $\pm$  2.0) > RG2  $(23.3^{\circ} \pm 1.5) > D2 (21.0^{\circ} \pm 0.8)$ . The results are comparable to the literature; 33–39° [81] for corn stalk fibers and 20° for sisal fibers [82]. Furthermore, a broad MFA distribution of 10–40° for sugarcane rinds has been reported [83]. The relation between an estimated MFA with FS and FM is presented in Figure 6b. The results demonstrated that both rind FS and FM properties decreased with MFA. It was reported that MFA affected both the rheological and mechanical properties of wood [84]. A larger MFA resulted in lower wood stiffness [85], which is consistent with our results. These results clearly show that

MFA is an important supramolecular structure of cellulose, affecting the biomechanical properties of lignocellulosic fibers. Despite the CI of RG2 being less than that of D1 (Table 4), the biomechanical property of RG2 was found to be significantly higher than D1. The biomechanical strength highly depends on the supramolecular network formed by complex carbohydrates and aromatic polymers [86]. Thus, the higher lignin content of RG2 could lead to stronger lignin–carbohydrate interaction and consequently higher biomechanical property (compared to D1). The stalk of RG2 was also different from D1 (Supplementary Figure S3). The morphological factors of maize have been reported to have a significant influence on its strength [87]. Microstructure and density also play a role in stalk strength [14,88].

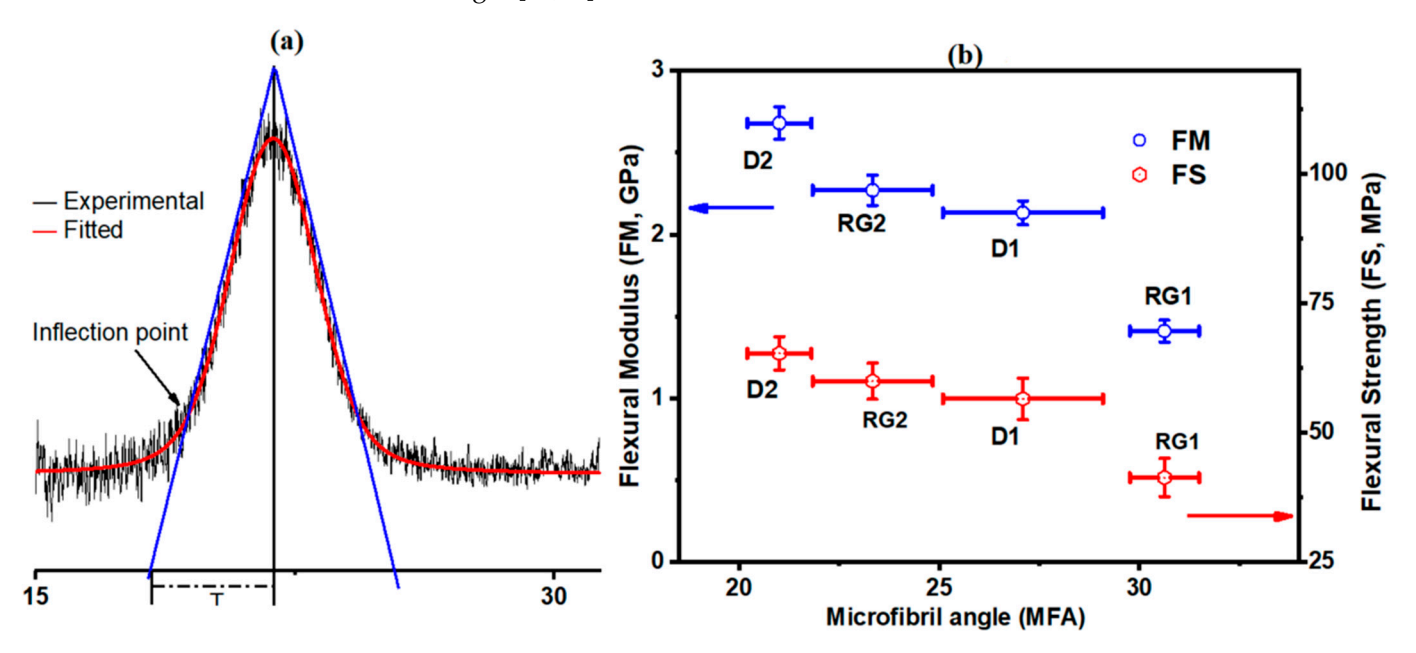


**Figure 6.** (a) Diffractogram of rind for determination of parameter T from (200); (b) relationship between MFA with flexural modulus (FM) and flexural strength (FS) determined from three-point micro-bending. Estimated MFA of each variety was determined from the average of five different IN1 rind specimens and reported with standard deviation (shown as error bars).

#### 2.5.3. Py-GCMS and DFRC Analysis

Py-GCMS, a thermal degradation technique that provides rapid in situ information on the cell wall constituents [89], was performed on the stalk rinds, and the pyrograms are presented in Supplementary Figure S4. The compositional variation in the IN1 rinds is revealed by the relative abundances of pyrolysis products, given in Supplementary Table S2. The whole cell walls released carbohydrate-derived compounds as well as lignin and p-hydroxycinnamates-derived phenolic compounds [90]. The pyrolysis products were consistent with the literature [91].

Lignin is a branched biopolymer composed mainly of coniferyl, sinapyl, and p-coumaryl alcohol monolignols which are respectively polymerized to guaiacyl (G), syringyl (S), and hydroxyphenyl (H) monomer units through dehydrogenative reactions [92]. The H, G, and S monomers differ in their degree of methoxylation, and the syringyl/guaiacyl (S/G) ratio determines extent of lignin cross-linking. The S/G ratio of the internode rind was determined from Py-GCMS data (Figure 7a). The S/G ratios were 0.29, 0.36, 0.34, and 0.38, respectively for D1, RG1, D2, and RG2, which was consistent with previous work [93]. The S/G ratios of RG1 and RG2 were significantly increased, respectively, by 24.1% and 11.4%. This result was consistent with previous reports of transgenic plants having an S/G ratio about 57% higher than wild-type maize plants [94]. The relative percentage of monolignols (H/G/S ratio) determined from Py-GC/MS (Figure 7b) showed that H lignin was the dominant monolignol (70–79%), consistent with the fact that p-coumaryl alcohol

(p-hydroxyphenyl)-derived lignin was more common in grasses [95]. The H/G/S ratios were 71/22/7 for D1, 79/15/6 for RG1, 70/22/8 for D2, and 69/23/8 for RG2. The detection of higher amounts of H lignin-derived compounds could be due to the degradation of p-coumaric (pCA) and ferulic (FA) phenolic acids to 4-vinylphenol. Furthermore, aromatic amino acid constituents of proteins in the rind may also contribute to the phenol peak.

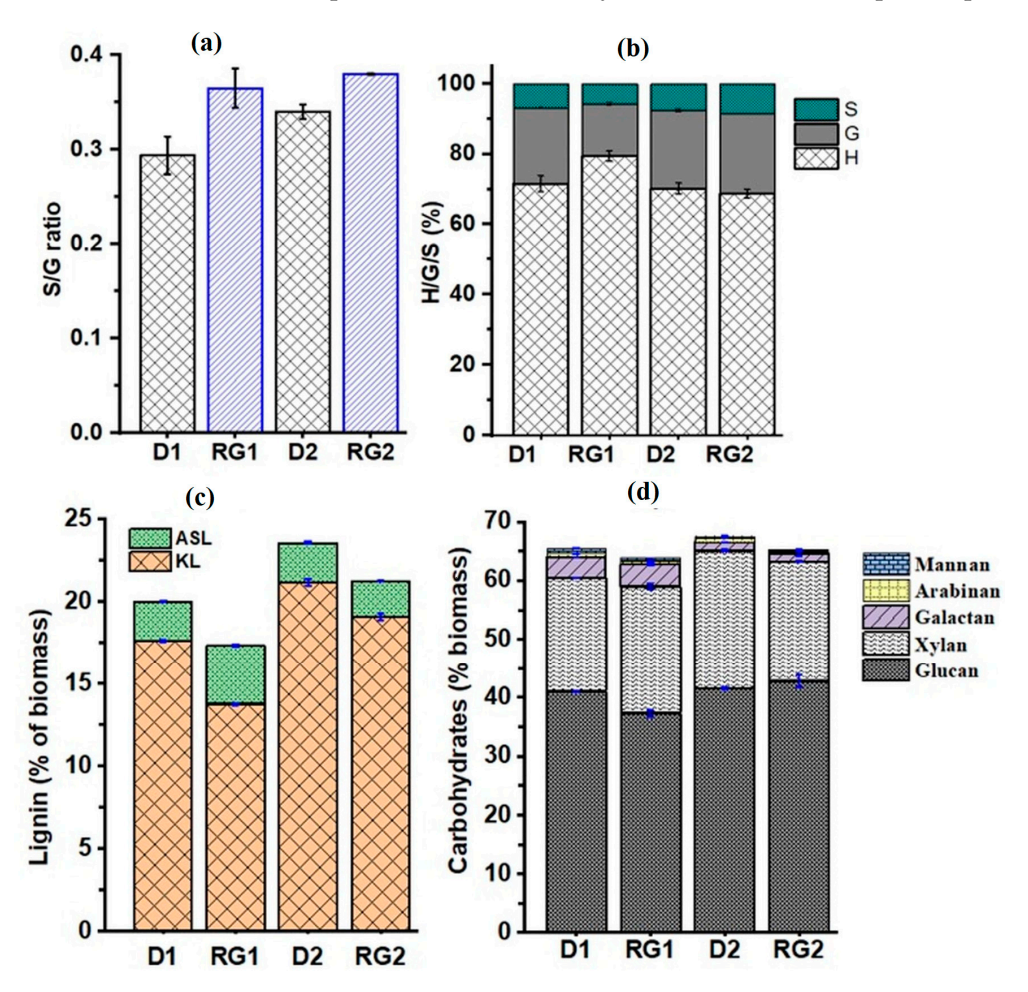


**Figure 7.** (a) S/G ratio comparison for D1, RG1, D2 and RG2 as determined by Py-GCMS; (b) relative percentage of monolignols (H/G/S, %) at the internodes; (c) lignin analysis: Klason Lignin (KL) and Acid Soluble Lignin (ASL); (d) carbohydrate analysis based on % of biomass.

The relative abundance of monolignols, their inter-linkages, the degree of polymerization, the number of free phenolic groups, and the degree of cross-linking with polysaccharides vary among different plant species, developmental stages, cell types, and plant tissue types [96]. The S/G ratio determines the extent of crosslinking in lignin. Technically, the presence of an extra methoxy group in lignin monomers gives one less linkage site (S < G < H), consequently leading to fewer coupling combinations during the polymerization reaction [97]. As S lignin has no vacant 5-position, cross-linkages such as  $\beta$ -5, 5,5', and 4-O-5 are not possible in S subunits. Thus, S-rich lignin was more easily depolymerized than G-rich lignin [97,98] yielding a less crosslinked lignin and more linear β-O-4 linkages [99]. The correlation between the bending properties (FM, FS) and lignin composition (Table 5) revealed that FS (r = 0.67) and FM (r = 0.73) were significantly and positively correlated with G lignin. This finding demonstrates that G lignin plays a significant role in enhancing the biomechanical properties and possible resistance against lodging. G lignin was reported to have a positive impact on lodging resistance in buckwheat [100]. Moreover, Wei et al. [101] and Li et al. [102] reported that G monolignol played an important role in lodging resistance. This could likely be related to the fact that greater G content leads

to highly crosslinked lignin due to the presence of a larger number of biphenyl and C-C linkages [99]. Contrarily, S lignin was not correlated with bending properties (Table 5). This result contradicts the literature [103], where S monomers were suggested to be the predominant structural lignin subunit for strength and rigidity in wheat plants. On the other hand, the pairwise correlation analysis showed that H lignin was negatively correlated (Table 5) with FS (r = -0.68) and FM (r = -0.72). It was reported that H-type lignin is deposited at an earlier stage, followed by G- and then S-type lignin units during lignification [104]. The higher H lignin in the RG variety suggests that the deposition of G-type and S-type lignin at later stages of lignification might be impaired by the mutation. Higher H-lignin was associated with reduced molecular weight and the biomass less recalcitrant [105]. However, according to Luo et al. [100], a higher proportion of H monomers were not important to the lodging resistance of wheat stems. On the other hand, a recent study [106] highlighted the importance of H lignin subunits in strengthening the maize stalk. One possible explanation is that H lignin detected in Py-GCMS could be both from canonical and non-canonical H lignin (pCA and FA). Thus, the exact effect of canonical H lignin on biomechanical properties might be interfering with the presence of phenolic acids. It was also shown (Table 5) that the S/G ratio was not correlated with either FM or FS. As the concentration of S lignin was variable across the varieties and growing seasons, thus the S/G ratio will undoubtedly have had no effect on stalk strength. A study in buckwheat demonstrated that the S/G ratio was not relevant for lodging resistance in different cultivars [100]. However, Ookawa et al. [30] reported that S/G was positively related to the flexural rigidity of rice stems. On the other hand, Wei et al. [101] reported that the S/G ratio exhibited a significant negative correlation with lodging resistance in oilseed crops. The limitation and inconsistency of the literature on the impact of lignin composition and cross-linkages on the biomechanical and lodging resistance properties of stalks has clearly indicated that further investigations using more varieties are needed in future study.

**Table 5.** Pearson's correlation coefficients between lignin composition (G, S and S/G) determined by Py-GCMS and bending properties (FS and FM) of sorghum rinds  $^1$ .

	FM	Н	G	S	S/G
FS	0.96 ***	-0.68 *	0.67 *	0.62	-0.17
FM		-0.72*	0.73 *	0.66	-0.20
Н			-0.99 **	-0.94 ***	0.16
G				0.89 **	-0.28
S					0.19

 $<sup>\</sup>overline{}^{1}$  H: p-hydroxyphenyl; G: guaiacyl; S: syringyl; S/G: syringyl/guaiacyl ratio; FS: Flexural strength; FM: flexural modulus. Symbols \*\*\*, \*\* and \* respectively represents significant correlation at p < 0.001, p < 0.01, and p < 0.05.

A DFRC is a degradation method that selectively cleaves  $\alpha$ - and  $\beta$ -ether linkages in lignin, releasing the lignin monomers involved in those linkages [107]. A characteristic and distinctive feature of the DFRC method in comparison with other degradative methods is that it leaves  $\gamma$ -esters intact, thus allowing the release of  $\gamma$ -acylated monolignols [89]. DFRC was performed on sorghum rinds and chromatograms of the degradation products are shown in Supplementary Figure S5. The results show that the lignin released both cis- and trans-isomers of p-hydroxyphenyl (cH and tH), guaiacyl (cG and tG), and syringyl (cS and tS) lignin monomers. The levels of monomers arising from the uncondensed arylglycerol β-aryl (β-O-4) ether linkage is given in Table 6. The results revealed that sorghum rind had HGS type lignin with a dominant G monolignol (Table 6). Significant variations in the β-ether linkage contents between the samples were found. Given that D2 had the highest lignin content, D2 also had the highest total uncondensed monomer released (4.25 mmol/g of lignin), followed by RG2 (3.44 mmol/g of lignin). D1 and RG1 had, respectively, 2.00 and 1.87 mmol/g of uncondensed monomer released. The total content of β-O-4-ethers for palm kernel lignin was reported at 2.29 mmol/g [108]. β-O-4 lignin linkages were the main linkages detected by 2D-NMR in sorghum stalks [93]. The data (Table 6) also indicated that

63–71% of  $\beta$ -O-4 were released as G monomer. Comparable S/G ratio for wheat straw has been reported [107].

**Table 6.** Relative molar abundance (mmol/g of lignin) of the DFRC degradation monomers of the MWL isolated from D2, RG2, D1, and RG1 sorghum stalks.

Rind Sample	H (mmol/g Lignin)	G (mmol/g Lignin)	S (mmol/g Lignin)	S/G	H/G/S	Total Yield (mmol/g Lignin)
D2	$0.39 \pm 0.04$	$2.68 \pm 0.06$	$1.18\pm0.04$	0.44	9/63/28	4.25
RG2	$0.37 \pm 0.02$	$2.25\pm0.02$	$0.81\pm0.05$	0.36	11/65/24	3.44
D1	$0.23 \pm 0.04$	$1.44\pm0.01$	$0.34 \pm 0.04$	0.24	12/71/17	2.00
RG1	$0.24\pm0.02$	$1.26\pm0.02$	$0.36\pm0.04$	0.29	13/68/19	1.87

#### 2.5.4. Lignin and Carbohydrate Analysis

Lignin and carbohydrate analyses were performed on IN1 rinds, and the results are given in Figure Figure 7c and Figure 7d, respectively. The Klason lignin (KL) content of the rinds (Figure 7c) was found to be 17.6%, 13.8%, 21.2%, and 19.1%, respectively, for D1, RG1, D2, and RG2. Meanwhile, the ASL contents were 2.40% for D1, 3.54% for RG1, 2.42% for D2, and 2.18% for RG2. The results were in close agreement with the whole cell wall of sorghum stalks previously reported [93]. A comparison of the results revealed that KL lignin was found to be significantly reduced by about 22.0 and 9.9% in RG1 and RG2 relative to D1 and D2, respectively. On the other hand, the acid soluble lignin (ASL) was 47.7% higher in RG1 relative to D1 but decreased by 10.0% in RG2 relative to D2. In comparison to Della, the total lignin content (KL + ASL) was significantly reduced by 13.6%. and 9.9%, respectively, for RG1 and RG2. Considering the significant reduction in the mechanical properties of RG1, this result suggests that lignin content may have a profound impact on mechanical properties. Across the growing season, the total lignin content of D2 and RG2 was about 17.9% and 22.9% higher than D1 and RG1, respectively. RG2 contained 6% higher total lignin than D1.

Carbohydrate analysis (Figure 7d) showed that glucan and xylan were the predominant components of the IN1 rind. The glucan/cellulose was 41.0%, 37.2%, 41.5%, and 42.8%, respectively, for D1, RG1, D2, and RG2. Similarly, the xylan/hemicellulose content was 19.5% for D1, 21.8% for RG1, 23.6% for D2, and 20.5% for RG2. Significant variations were particularly detected between D1 and RG1, with a 9.0% glucan reduction and a 11.8% increase in xylan. On the other hand, the glucan content of D2 and RG2 was similar, although a 13.1% reduction in xylan was detected in RG2. It was reported that cellulose and lignin concentration in sorghum was highly affected by growing seasons and environmental factors [109], which corroborates our finding that changes in lignin and carbohydrate content were likely related to seasonal variations. Other minor components like mannan, arabinan, and galactan were also detected as shown in Figure 7d. Previous studies [110,111] have shown that the biomechanical properties of the biomass tissues are highly correlated with composition. A significant reduction in lignin and glucan in RG could be due to reduced lignin and cellulose deposition in the sclerenchyma and vascular bundle cells [112]. This may consequently lead to weak tissue and low stem strength, causing a higher degree of lodging incidence.

## 2.6. Correlations of Chemical Compositions with Flexural Properties

The cell wall composition of lignocellulosic material has a significant effect on its macro-scale mechanical behavior [27], which can be attributed to the cell wall micro-structure and chemical differences. The effect of chemical composition on the bending properties of the stalks has been evaluated, and their Pearson's correlation coefficients are shown in Table 7. It was found that FS and FM were significantly correlated with KL, ASL, and glucan/cellulose content. The results revealed that FS had a strong positive correlation with KL (r = 0.88), TL (r = 0.86), and cellulose content (r = 0.70) but were

negatively correlated with ASL (r = -0.70). Similarly, for FM significant correlations with KL (r = 0.82), TL (r = 0.81), and cellulose (r = 0.68) were observed. These findings have been well supported in the literature, where lignin content played a key role in a significant improvement in mechanical properties, eventually enhancing the lodging resistance of crops [113-115]. Compared to lodging-resistant varieties, low lignin content was detected in lodging-type wheat, rice, corn, and miscanthus [100,116–119]. Reductions in lignin content were also associated with reductions in FS and FM in poplar wood [120]. Cellulose constitutes the main backbone of the cell wall, and its content and structure contribute to the stiffness and strength of the cell wall. Stalk breaking resistance has been found to be positively correlated with the cellulose and lignin content of maize internodes [121]. Kobubo et al. [12] found a positive correlation between FS and cellulose content. Moreover, a significant correlation of FM with cellulose content (r = 0.79) and lignin content (r = 0.47) has been reported in young bamboo [111]. On the other hand, bending properties were not significantly correlated with hemicellulose content, similar to the reports on bamboo [111]. The hemicelluloses content was not significantly correlated with breaking force in rice, which is an important indicator of stem lodging [122]. Contrarily, bending strength was found to decrease with ASL content (r = -0.70) (Table 7). Nevertheless, no published data were found about the correlation of bending behavior with ASL content. The results clearly demonstrated that rind biomechanical properties were strongly correlated with their chemical composition and that a low content of lignin and cellulose results in weak stem strength and could easily cause stem lodging [37].

**Table 7.** Pearson's correlation coefficients between chemical composition and bending properties <sup>1</sup>.

	FM	KL	ASL	TL	Glucan/Cellulose	Hemicellulose
FS	0.96 ***	0.88 ***	-0.78 ***	0.86 ***	0.70 ***	-0.35
FM		0.82 ***	-0.70***	0.81 **	0.68 ***	-0.25
KL			-0.76 **	0.99 ***	0.67 ***	-0.30
ASL				-0.69***	-0.48 **	0.57
TL					0.68 ***	-0.22
Cellulose						-0.62

 $<sup>\</sup>overline{\phantom{a}}$  Klason lignin (KL), acid soluble lignin (ASL), total lignin (TL) and cellulose; with flexural strength (FS) and flexural modulus (FM) at internodes in sorghum; \*\*\*, and \*\* represent significant correlation respectively at p < 0.001 and p < 0.01.

## 3. Materials and Methods

## 3.1. Plant Material

Sweet sorghum stalks were collected from the University of Kentucky Horticulture Research Farm (Emmitt Road, Lexington, KY, USA) during the 2018 (Della1, RG1) and 2019 (Della 2, RG2) growing seasons [123], shown in Supplementary Figure S4. RG is an acronym for *REDforGREEN* mutant variety. Samples of four matured stalks were pooled for each variety in both years. The rind from the internodes was sectioned out using a razor blade, and residual pith on the inner surface was removed and smoothed (Figure 8a). The thickness and width of the rinds at internodes were measured using a micrometer and a caliper, respectively.

#### 3.2. Mechanical and Viscoelastic Properties

The viscoelastic and biomechanical properties of sectioned internode rind specimens were investigated using a Q800 DMA (TA Instruments) in three-point bending (10 mm span) (Figure 8b,c).

## 3.2.1. Micro-Biomechanical Bending Tests

All micro-biomechanical bending tests were performed on rind tissues of stalk samples (at ambient conditions and ~4% moisture content). Two individual stalks from either genotype across both years were selected, and rind tissues were sectioned from IN1-IN5

(Figure 1a). At each internode, at least eight technical replicates of rind tissue (approximately  $14 \times 3.6 \times 1.1 \text{ mm}^3$ ) were collected and tested at a strain rate of  $0.5\% \cdot \text{min}^{-1}$  to a final strain of 6%, until failure was detected. Data were analyzed by TA analysis software, and the stress–strain curves and flexural properties (FM and FS) were determined.

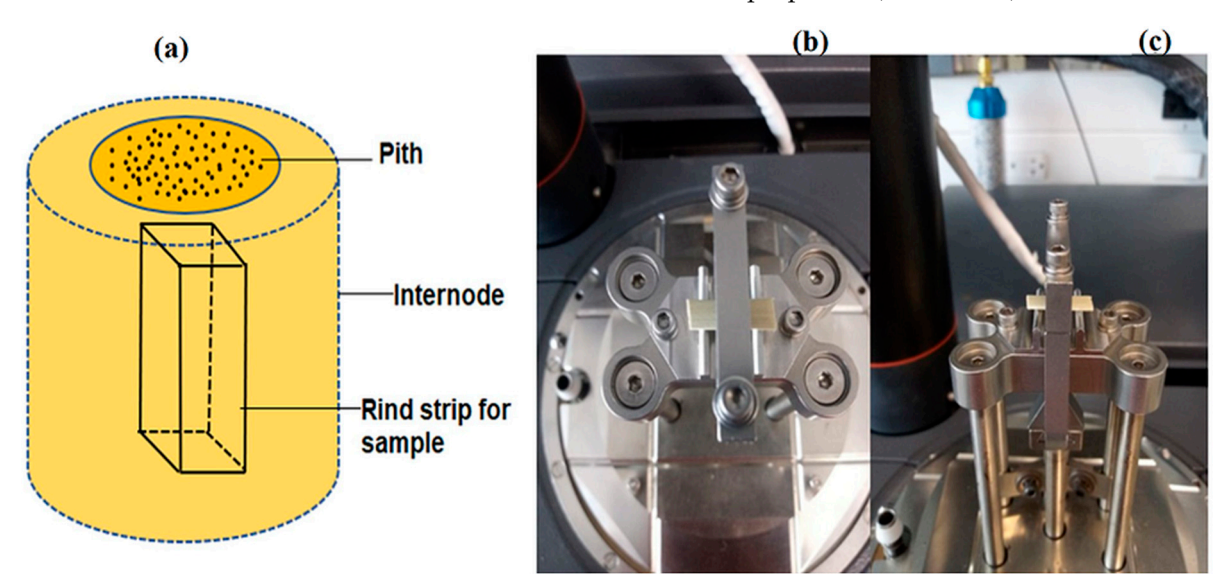


**Figure 8.** Experimental setup for DMA tests; (a) depiction of rind specimen sectioned from stalk internodes; (b) rind specimen in the 3-point bending fixture—top view; and (c) rind specimen in the 3-point bending fixture—side view.

#### 3.2.2. Viscoelastic Properties Response to Relative Humidity

The viscoelastic parameters (storage modulus (E", loss modulus (E'), and tan  $\delta$ )) of IN1 stalk rinds (approximately  $10 \times 4 \times 1.5 \text{ mm}^3$ ), in triplicate, were also investigated using the DMA in three-point bending mode (1% strain). All samples were subjected to a relative humidity (RH) ramp (0 to 80%) at ambient temperature with a rate of  $2\% \cdot \text{min}^{-1}$ . The viscoelastic properties of the sorghum rinds were evaluated as a function of RH.

## 3.2.3. Stress Relaxation

The stress relaxation behavior of the IN1 rind specimen (approximately  $12 \times 4 \times 1.5 \text{ mm}^3$  rind) was determined using the DMA in three-point bending mode by applying a constant strain of 5% throughout the experiment and measuring the corresponding stress required to maintain the deformation as a function of time for 15 min. At least 10 replicates were tested for each sample. The relaxation modulus E(t) was described according to the generalized Maxwell model (GMM) [124] as:

$$E(t) = E_{\infty} + \sum_{i=1}^{n} E_{i} \exp\left(\frac{-E_{i}t}{\eta_{i}}\right) = E_{\infty} + \sum_{i=1}^{n} E_{i} \exp\left(\frac{-t}{\tau_{i}}\right)$$
(1)

where E(t) is relaxation modulus at time t. At long times the cell wall polymer molecules start to gradually accommodate the strain by conformational extension rather than bond distortion, and the E(t) falls exponentially to a lower equilibrium modulus  $\lim_{t\to\infty} E(t) = E_{\infty}$ .  $E_i$  is the relaxation modulus parameter,  $\eta_i$  is the viscosity of the dashpot for the ith series, n is the number of springs–dashpot, and  $\tau_i = \eta_i/E_i$  is relaxation time.

## 3.2.4. Creep Behavior

Creep is the slow continuous deformation of a material under constant stress. The creep behavior of the IN1 stalk rind (approximately  $12 \times 3.6 \times 1.1 \text{ mm}^3$ ) was determined by DMA in three-point bending mode with a constant stress of 40 MPa exerted for 15 min at ambient temperature, and creep dynamical change was recorded. A preload force of 0.001 N

was applied. At least 10 replicates were tested for each sample. The creep compliance C(t) was modelled according to the generalized Kelvin model (GKM) [125] as:

$$C(t) = C_0 + C_1 \left( 1 - \exp\left(\frac{-t}{\tau_1}\right) \right) + C_2 \left( 1 - \exp\left(\frac{-t}{\tau_2}\right) \right) \tag{2}$$

where  $C_0$  is initial compliance,  $C_1$ , and  $C_2$  are model coefficients, and  $\tau_1$  and  $\tau_2$  are retardation times.

## 3.2.5. Viscoelastic Properties Response to Temperature

The viscoelastic properties of the IN1 stalk rind (approximately  $12 \times 4.0 \times 1.6$  mm³), in triplicate, were determined using a temperature sweep (25 °C to 120 °C at 3 °C·min<sup>-1</sup>) in three-point bending mode with a constant strain of 1% and frequency of 1 Hz. Prior to the experiment, the rind specimen was equilibrated at 80% RH for 4 h. The softening temperature was measured from the peak of the loss modulus (E") and tan  $\delta$ .

# 3.3. Compositional Analysis

After testing the biomechanical and viscoelastic properties, the rinds were collected for further compositional analysis using different analytical techniques.

# 3.3.1. Fourier-Transform Infrared (FTIR) Spectroscopy

FTIR spectra were obtained on previously three-point bend-tested IN1 specimens in triplicate using an iS5 spectrometer (Thermo-Nicolet, Madison, WI, USA) equipped with a ZnSe attenuated total reflection (iD5 ATR) accessory. The spectra were averaged, baseline corrected and normalized to the highest band (1032 cm<sup>-1</sup>, cellulose) using the Omnic v9 software.

#### 3.3.2. Lignin and Carbohydrate Analysis

Extractive-free IN1 rind samples (200 mg) were hydrolyzed using sulfuric acid (2 mL, 72%) for 60 min at 30 °C in water bath followed by secondary hydrolysis (4% sulfuric acid, 30 min, 20 psi) in an autoclave according to a modified ASTM D 1106-96. The Klason lignin (KL) content was determined gravimetrically after filtration, whereas acid soluble lignin (ASL) was determined by UV/Vis spectroscopy (Genesys 50, ThermoScientific, Madison, WI, USA) at 205 nm using an absorption coefficient of 110 L g $^{-1}$  cm $^{-1}$  [126]. Structural carbohydrate analysis was performed on the hydrolyzed filtrate (5 mL), with the addition of mannitol as an internal standard, according to ASTM E 1758-01. The sugars were separated and quantified using high-performance liquid chromatography (HPLC, two Rezex RPM columns, 7.8 mm  $\times$  30 mm, Phenomenex, Torrance, CA, USA) at 85 °C on elution with water (0.5 mL·min $^{-1}$ ) using differential refractive index detection (Waters model 2414). Cellulose was estimated as the equivalent of glucose concentration, whereas hemicellulose was estimated from the summation of xylose, galactose, arabinose, and mannose monomers.

## 3.3.3. Microfibril Angle by XRD

X-ray diffraction (XRD) analysis for crystallinity index (CI) was performed on milled three-point bend-tested specimens of IN1-IN5 (5 samples, one sample from each internode) using a Siemens D5000 diffractometer using Cu K $\alpha$  radiation ( $\lambda$  = 0.154 nm) from 2 $\theta$  = 2 to 80° at 0.05° steps. After the deconvolution of the amorphous and crystalline regions using Gaussian curve-fitting, the CI based on area and the grain size of cellulose at (200) were determined [73,93].

The MFA of cellulose in the fibrovascular bundles on the exterior side of a three-point bend-tested IN1 rind specimen was estimated using a Bruker D8 Discover XRD equipped with an array detector (GADDS). The data were collected using Cu-K $\alpha$  radiation operating

at 40 kV and 20 mA, and the area was integrated using the DIFFRAC.EVA software. MFA was determined according to the works of Yamamoto et al. [127] as:

$$MFA = 1.575 \times 10^{-3} \, T^3 - 1.431 \times 10^{-1} \, T^2 + 4.693T - 36.19$$
 (3)

The diffractograms were corrected to obtain the parameter T value of (200) [128]. The baseline of the diffractograms was subtracted. Then, the reflection profiles were separated, and the T value was determined from second derivatives of (200) profiles (Figure 6a). The description of the method is given by de Souza et al. [80] and Rekha [129].

## 3.3.4. Analytical Py-GCMS Analysis

The p-hydroxyphenyl (H)/G/S ratio was determined on IN1 specimens by pyrolysis–GCMS (Py-GCMS) using a Pyrojector II unit (SGE Analytical Science, Melbourne, Australia) at 500 °C coupled to a GC-MS (ISQ-Trace1300, ThermoScientific). The compounds were separated using ZB-5 capillary column (30 m × 0.25 mm Ø, 0.25 µm coating, Phenomenex) from 50 °C (1 min) to 250 °C (10 min) at 5 °C·min<sup>-1</sup>. Compounds were identified by comparison with standards, the literature [130], and the NIST-2017 mass spectral library. The H/G/S ratio was determined from peak areas of lignin monomers by a selective ion monitoring chromatogram for H for 7–15 min (m/z = 94, 107, 108, 120, 121, 134, 148), G for 18–23 min (m/z = 124, 135, 137, 138, 151, 164, 178), and S for 24–28 min (m/z = 154, 165, 167, 168, 181, 194, 208) [131].

#### 3.3.5. Derivatization Followed by Reductive Cleavage (DFRC)

The frequency of lignin  $\beta$ -ether bonds in the IN1 stalk rind was determined using the DFRC method according to the protocol of Lu and Ralph [132] with slight modification. Sorghum rind samples (20 mg) were derivatized and solubilized with an acetic acid/acetyl bromide solution (4:1 v/v, 5 mL) upon stirring at 50 °C for 1 h; then, acetyl bromide was removed under vacuum. The solid residue was dispersed in dioxane/acetic acid/water (5.4.1 v/v, 5 mL), zinc powder (50 mg) was added, and the mixture was stirred for 30 min at room temperature. The zinc powder was removed by filtration, and tetracosane (10 mg in dichloromethane (CH<sub>2</sub>Cl<sub>2</sub>, 10 mL)) was added as internal standard to the filtrate. The organic layer was washed with saturated NH<sub>4</sub>Cl, and recovered, then the aqueous layer was further extracted using CH<sub>2</sub>Cl<sub>2</sub> (10 mL). The combined extracts were dried over anhydrous NaSO<sub>4</sub> and concentrated to dryness. Finally, the sample was acetylated with acetic acid/pyridine (1:1 v/v, 2 mL) at room temperature for 40 min, reaction quenched with ethanol and excess reagents were removed under vacuum. The solid residue was dissolved in CH<sub>2</sub>Cl<sub>2</sub> (1.5 mL) and analyzed by electron impact GC-MS (ISQ7000-Trace1300, ThermoScientific, Madison, WI, USA). Separation was achieved using a ZB-1ms capillary column (30 m  $\times$  0.25 mm i.d, Phenomenex) and temperature program of 100  $^{\circ}$ C (1 min) to  $300~^{\circ}\text{C}$  (1 min) at  $5~^{\circ}\text{C}\cdot\text{min}^{-1}$ . The quantification and characterization of DFRC products was performed according to the literature and using response factors of 1.76, 1.85, and 2.06, respectively, for H, G, and S [133].

## 3.3.6. Statistical Analysis

The stalk rinds were not geometrically flawless due to their irregular shape. Thus, geometrically smoothed samples were taken at each internode (at least eight replicates) and tested. The standard deviation was used to measure reproducibility for each specimen. One-way analysis of variance (ANOVA) was used to find differences in properties between the varieties at the internodes, where a 95% (p = 0.05) confidence level was used to assess statistical significance.

#### 4. Conclusions

The rind mechanical and viscoelastic properties of Della and RG sorghum stalk varieties grown in two different seasons have been evaluated using DMA. The three-point bending test results have provided two useful quantities: flexural modulus (FM) and

flexural strength (FS). The results have shown that a significant reduction in FM and FS is associated with lignin and cellulose content reduction. Particularly, the FS and FM values of the RG2 variety have been found to be significantly reduced and attributed to low lignin and cellulose contents. Acid soluble lignin has been found to be negatively correlated, whereas Klason lignin is positively correlated with biomechanical properties. However, hemicellulose was not shown to significantly influence mechanical properties. The combined influence of lignin and cellulose content shows the most significant effect on both the FM and FS. Furthermore, MFA was an important superstructural parameter, highly influencing biomechanical property. This study further suggests that varieties with lower MFA and higher lignin and cellulose accumulation can further be used for breeding to develop lodging resistance cultivars. DMA using a three-point micro-bending fixture has been shown to be a convenient and efficient tool for measuring mechanical properties of crop stalk rind sections at a small scale.

Supplementary Materials: The following supporting information can be downloaded at: https://www.mdpi.com/article/10.3390/crops4010002/s1, Figure S1: XRD diffractograms of powdered sorghum rinds from D2, RG2, D1 and RG1. The diffraction was performed on the powder samples of rinds. The diffractogram shown is obtained after subtracting the baseline and deconvolution of the amorphous and crystalline regions using Gaussian curve-fitting. The peaks (110) and (1–10) were not detected as separate peaks; Figure S2: X-ray diffraction patterns of intact D2, RG2, D1 and RG1 rinds; Figure S3: Representative samples for RG1, D1, RG2 and D2 stalks at Internode 2; Figure S4: Py-GCMS pyrograms of rinds from (a) D2, (b) RG2, (c) D1 and (d) RG1; Figure S5: Chromatograms (GC-TIC) of the DFRC degradation products from the MWL isolated from sorghum stalks of: (a) D2, (b) RG2, (c) D1 and (d) RG1. The monomers cH, tH, cG, tG, cS, represents cis- and trans- p-hydroxyphenyl, guaiacyl and syringyl; Table S1: FTIR Assignments for functional groups in sorghum rinds of WT1, RG1, WT2 and RG2 assigned based on [71,93]; Table S2: Pyrolysis products identified in the rinds of D2, RG2, D1 and RG1 sorghum variety.

**Author Contributions:** Conceptualization, A.G.M., S.D. and E.M.; methodology, A.G.M. and E.M.; validation, A.G.M., S.D. and E.M.; formal analysis, E.M.; investigation, E.M. and A.G.M.; resources, N.B. and S.D.; data curation, E.M.; writing—original draft preparation, E.M. and A.G.M.; writing—review and editing, A.G.M., N.B., S.D. and E.M.; visualization, E.M; supervision, A.G.M.; project administration, A.G.M. and S.D.; funding acquisition, S.D. All authors have read and agreed to the published version of the manuscript.

Funding: This research was funded by the National Science Foundation grant number 1826715.

**Data Availability Statement:** All data generated or analyzed during this study are included in this published article and its supplementary information files.

**Acknowledgments:** The authors would like to acknowledge (i) the University of Idaho Equipment and Infrastructure Support (EIS) Awards Program from the Office of Research and Economic Development (ORED) RISE Funding Program and the College of Natural Resources to support the purchase of the GCMS, (ii) USDA-CSREES grant 2007-34158-17640 for support in the purchase of the DMA and (iii) Thomas Williams for helping with the XRD analyses.

**Conflicts of Interest:** The funders had no role in the design of the study; in the collection, analyses, or interpretation of data; in the writing of the manuscript; or in the decision to publish the results.

#### References

- 1. Gomez, F.; Mullet, J.; Muliana, A.; Niklas, K.; Rooney, W. The genetic architecture of biomechanical traits in sorghum. *Crop Sci.* **2020**, *60*, 82–99. [CrossRef]
- 2. Wu, W.; Ma, B. A new method for assessing plant lodging and the impact of management options on lodging in canola crop production. *Sci. Rep.* **2016**, *6*, 31890. [CrossRef]
- 3. Shah, L.; Yahya, M.; Shah, A.; Nadeem, M.; Ali, A.; Wang, J.; Riaz, W.; Rehman, S.; Wu, W.; Khan, M.; et al. Improving Lodging Resistance: Using Wheat and Rice as Classical Examples. *Int. J. Mol. Sci.* **2019**, 20, 4211. [CrossRef] [PubMed]
- 4. Shah, N.; Tanveer, M.; Rehman, A.; Anjum, S.; Iqbal, J.; Ahmad, R. Lodging stress in cereal—Effects and management: An overview. *Environ. Sci. Pollut. Res.* **2017**, 24, 5222–5237. [CrossRef] [PubMed]

5. Hu, H.; Liu, W.; Fu, Z.; Homann, L.; Technow, F.; Wang, H.; Song, C.; Li, S.; Melchinger, A.; Chen, S. QTL mapping of stalk bending strength in a recombinant inbred line maize population. *Theor. Appl. Genet.* **2013**, 126, 2257–2266. [CrossRef]

- 6. Brulé, V.; Rafsanjani, A.; Pasini, D.; Western, T. Hierarchies of plant stiffness. Plant Sci. 2016, 250, 79–96. [CrossRef]
- 7. Speck, T.; Burgert, I. Plant Stems: Functional Design and Mechanics. Annu. Rev. Mater. Res. 2011, 41, 169–193. [CrossRef]
- 8. Bayable, M.; Tsunekawa, A.; Haregeweyn, N.; Ishii, T.; Alemayehu, G.; Tsubo, M.; Adgo, E.; Tassew, A.; Tsuji, W.; Asaregew, F.; et al. Biomechanical Properties and Agro-Morphological Traits for Improved Lodging Resistance in Ethiopian Teff (*Eragrostis tef* (Zucc.) Trottor) Accessions. *Agronomy* **2020**, *10*, 1012. [CrossRef]
- 9. Khobra, R.; Sareen, S.; Meena, B.; Kumar, A.; Tiwari, V.; Singh, G. Exploring the traits for lodging tolerance in wheat genotypes: A review. *Physiol. Mol. Biol. Plants* **2019**, 25, 589–600. [CrossRef]
- 10. Shah, N.; Tanveer, M.; Abbas, A.; Yildirim, M.; Shah, A.; Ahmad, I.; Wang, Z.; Sun, W.; Song, Y. Combating Dual Challenges in Maize Under High Planting Density: Stem Lodging and Kernel Abortion. *Front. Plant Sci.* **2021**, *12*, 699085. [CrossRef]
- 11. Kong, E.; Liu, D.; Guo, X.; Yang, W.; Sun, J.; Li, X.; Zhan, K.; Cui, D.; Lin, J.; Zhang, A. Anatomical and chemical characteristics associated with lodging resistance in wheat. *Crop J.* **2013**, *1*, 43–49. [CrossRef]
- 12. Kokubo, A.; Kuraishi, S.; Sakurai, N. Culm Strength of Barley Correlation Among Maximum Bending Stress, Cell Wall Dimensions, and Cellulose Content. *Plant Physiol.* **1989**, *91*, 876–882. [CrossRef] [PubMed]
- 13. Zhong, R.; Ye, Z. Secondary Cell Walls: Biosynthesis, Patterned Deposition and Transcriptional Regulation. *Plant Cell Physiol.* **2015**, *56*, 195–214. [CrossRef] [PubMed]
- 14. Shah, D.; Reynolds, T.; Ramage, M. The strength of plants: Theory and experimental methods to measure the mechanical properties of stems. *J. Exp. Bot.* **2017**, *68*, 4497–4516. [CrossRef] [PubMed]
- 15. Yang, S.; Xie, L.; Zheng, S.; Li, J.; Yuan, J. Effects of Nitrogen Rate and Transplanting Density on Physical and Chemical Characteristics and Lodging Resistance of Culms in Hybrid Rice. *Acta Agron. Sin.* **2009**, *35*, 93–103. [CrossRef]
- Luyckx, M.; Hausman, J.; Lutts, S.; Guerriero, G. Silicon and plants: Current knowledge and technological perspectives. Front. Plant Sci. 2017, 8, 411. [CrossRef]
- 17. Lee, S.; Zargar, O.; Reiser, C.; Li, Q.; Muliana, A.; Finlayson, S.; Gomez, F.; Pharr, M. Time-dependent mechanical behavior of sweet sorghum stems. *J. Mech. Behav. Biomed. Mater.* **2020**, *106*, 103731. [CrossRef]
- 18. Gomez, E.; Muliana, A.; Niklas, K.; Rooney, W. Identifying Morphological and Mechanical Traits Associated with Stem Lodging in Bioenergy Sorghum (*Sorghum bicolor*). *Bioenergy Res.* **2017**, *10*, 635–647. [CrossRef]
- 19. Cosgrove, J.; Jarvis, C. Comparative structure and biomechanics of plant primary and secondary cell walls. *Front. Plant Sci.* **2012**, 3, 204. [CrossRef]
- 20. Wu, W.; Ma, B. The mechanical roles of the clasping leaf sheath in cereals: Two case studies from oat and wheat plants. *J. Agron. Crop Sci.* **2020**, 206, 118–129. [CrossRef]
- 21. Zuber, M.; Colbert, T.; Darrah, L. Effect of Recurrent Selection for Crushing Strength on Several Stalk Components in Maize. *Crop Sci.* **1980**, *20*, 711–717. [CrossRef]
- 22. Peiffer, J.; Flint-Garcia, S.; De Leon, N.; McMullen, M.; Kaeppler, S.; Buckler, E. The Genetic Architecture of Maize Stalk Strength. *PLoS ONE* **2013**, *8*, e67066. [CrossRef]
- 23. Arzola-Villegas, X.; Lakes, R.; Plaza, N.; Jakes, J. Wood Moisture-Induced Swelling at the Cellular Scale—Ab Intra. *Forests* **2019**, 10, 996. [CrossRef]
- 24. Lyu, J.; Peng, H.; Cao, J.; Jiang, J.; Zhao, R.; Gao, Y. Application of dynamic mechanical analysis in wood science research. *J. For. Eng.* **2018**, *3*, 1–11.
- 25. Chen, H.; Zhao, N.; Fu, N.; Li, D.; Wang, J.; Chen, D. Mechanical Properties of Hulless Barley Stem with Different Moisture Contents. *Int. J. Food Eng.* **2019**, *15*, 20180033. [CrossRef]
- 26. Erndwein, L.; Cook, D.; Robertson, D.; Sparks, E. Field-based mechanical phenotyping of cereal crops to assess lodging resistance. *Appl. Plant Sci.* **2020**, *8*, e11382. [CrossRef]
- 27. Winandy, J.; Rowell, R. The Chemistry of Wood Strength. In *The Chemistry of Solid Wood*, 1st ed.; Rowell, R., Ed.; American Chemical Society: Washington, DC, USA, 1984; pp. 211–255.
- 28. Stubbs, C.; Oduntan, Y.; Keep, T.; Noble, S.; Robertson, D. The effect of plant weight on estimations of stalk lodging resistance. *Plant Methods* **2020**, *16*, 28. [CrossRef] [PubMed]
- 29. Martin-Nelson, N.; Sutherland, B.; Yancey, M.; Liao, C.; Stubbs, C.; Cook, D. Axial variation in flexural stiffness of plant stem segments: Measurement methods and the influence of measurement uncertainty. *Plant Methods* **2021**, *17*, 101. [CrossRef]
- 30. Ookawa, T.; Yasuda, K.; Kato, H.; Sakai, M.; Seto, M.; Sunaga, K.; Motobayashi, T.; Tojo, S.; Hirasawa, T. Biomass production and lodging resistance in "Leaf Star", a new long-culm rice forage cultivar. *J. Plant Prod. Sci.* **2009**, *13*, 58–66. [CrossRef]
- 31. Li, M.; Yan, G.; Bhalla, A.; Maldonado-Pereira, L.; Russell, P.; Ding, S.; Mullet, J.; Hodge, D. Physical fractionation of sweet sorghum and forage/energy sorghum for optimal processing in a biorefinery. *Ind. Crops Prod.* **2018**, 124, 607–616. [CrossRef]
- 32. Gomez, F.; Muliana, A.; Rooney, W. Predicting Stem Strength in Diverse Bioenergy Sorghum Genotypes. *Crop Sci.* **2018**, *58*, 739–751. [CrossRef]
- 33. Wright, C.; Pryfogle, P.; Stevens, N.; Steffler, E.; Hess, J.; Ulrich, T. Biomechanics of Wheat/Barley Straw and Corn Stover. *Appl. Biochem. Biotechnol.* **2005**, 121–124, 5–20. [CrossRef]
- 34. Robertson, D.; Lee, S.; Julias, M.; Cook, D. Maize Stalk Lodging: Flexural Stiffness Predicts Strength. *Crop Sci.* **2016**, *56*, 1711–1718. [CrossRef]

- 35. Zhang, L.; Yang, Z.; Zhang, Q.; Guo, H. Tensile properties of maize stalk rind. BioResources 2016, 11, 6151–6161. [CrossRef]
- 36. Xu, Y.; Li, J.; Xin, Z.; Bean, S.; Tilley, M.; Wang, D. Water-soluble sugars of pedigreed sorghum mutant stalks and their recovery after pretreatment. *Appl. Sci.* **2020**, *10*, 5472. [CrossRef]
- 37. Sekhon, R.; Joyner, C.; Ackerman, A.; McMahan, C.; Cook, D.; Robertson, D. Stalk Bending Strength is Strongly Associated with Maize Stalk Lodging Incidence Across Multiple Environments. *Field Crops Res.* **2020**, 249, 107737. [CrossRef]
- 38. Esechie, H.; Maranville, J.; Ross, W. Relationship of Stalk Morphology and Chemical Composition to Lodging Resistance in Sorghum. *Crop Sci.* **1977**, *17*, 609–612. [CrossRef]
- 39. Hansen, S.; Ray, P.; Karlsson, A.; Jorgensen, B.; Borkhardt, B.; Petersen, B.; Ulvskov, P. Mechanical Properties of Plant Cell Walls Probed by Relaxation Spectra. *Plant Physiol.* **2011**, *155*, 246–258. [CrossRef]
- 40. Zhan, T.; Jiang, J.; Lu, J.; Peng, H. Dynamic viscoelastic properties of Chinese fir under cyclical relative humidity variation. *J. Wood Sci.* **2015**, *61*, 465–473. [CrossRef]
- 41. Czibula, C.; Seidlhofer, T.; Ganser, C.; Hirn, U.; Teichert, C. Longitudinal and transverse low frequency viscoelastic characterization of wood pulp fibers at different relative humidity. *Materialia* **2021**, *16*, 101094. [CrossRef]
- 42. Jakes, J. Mechanism for Diffusion through Secondary Cell Walls in Lignocellulosic Biomass. *J. Phys. Chem. B* **2019**, 123, 4333–4339. [CrossRef] [PubMed]
- 43. Zauscher, S.; Caulfield, D.; Nissan, A. The influence of water on the elastic modulus of paper. Part I: Extension of the H-bond theory. *Tappi J.* **1996**, *79*, 178–182.
- 44. Meng, Y.; Xia, Y.; Young, T.; Cai, Z.; Wang, S. Viscoelasticity of wood cell walls with different moisture content as measured by nanoindentation. *RSC Adv.* **2015**, *5*, 47538–47547. [CrossRef]
- 45. Birkinshaw, C.; Buggy, M.; Henn, G. Dynamic mechanical analysis of wood. J. Mater. Sci. Lett. 1986, 5, 898–900. [CrossRef]
- 46. Kaboorani, A.; Blanchet, P. Determining the linear viscoelastic region of sugar maple wood by dynamic mechanical analysis. *BioResources* **2014**, *9*, 4392–4409. [CrossRef]
- 47. Zhang, T.; Bai, S.; Zhang, Y.; Thibaut, B. Viscoelastic properties of wood materials characterized by nanoindentation experiments. *Wood Sci. Technol.* **2012**, *46*, 1003–1016. [CrossRef]
- 48. Kong, L.; Zhao, Z.; He, Z.; Yi, S. Effects of steaming treatment on crystallinity and glass transition temperature of *Eucalyptuses grandis* × *E. urophylla. Results Phys.* **2017**, *7*, 914–919. [CrossRef]
- 49. Wan, G.; Frazier, T.; Jorgensen, J.; Zhao, B.; Frazier, C. Rheology of transgenic switchgrass reveals practical aspects of biomass processing. *Biotechnol. Biofuels* **2018**, *11*, 57. [CrossRef]
- 50. Cristea, M.; Ionita, D.; Iftime, M. Dynamic Mechanical Analysis Investigations of PLA-Based Renewable Materials: How Are They Useful? *Materials* **2020**, *13*, 5302. [CrossRef]
- 51. Horvath, B.; Peralta, P.; Frazier, C.; Peszlen, I. Thermal softening of transgenic aspen. *BioResources* 2011, 6, 2125–2134. [CrossRef]
- 52. Stelte, W.; Clemons, C.; Holm, J.; Ahrenfeldt, J.; Henriksen, U.; Sanadi, A. Thermal transitions of the amorphous polymers in wheat straw. *Ind. Crops Prod.* **2011**, *34*, 1053–1056. [CrossRef]
- 53. Olsson, A.; Salmén, L. The effect of lignin composition on the viscoelastic properties of wood. *Nord. Pulp Paper Res. J.* **1997**, 12, 140–144. [CrossRef]
- 54. Chowdhury, S.; Frazier, E. Thermorheological complexity and fragility in plasticized lignocellulose. *Biomacromolecules* **2013**, *14*, 1166–1173. [CrossRef]
- 55. Börcsök, Z.; Pásztory, Z. The role of lignin in wood working processes using elevated temperatures: An abbreviated literature survey. *Eur. J. Wood Prod.* **2020**, *79*, 511–526. [CrossRef]
- 56. Chowdhury, S.; Fabiyi, J.; Frazier, E. Advancing the dynamic mechanical analysis of biomass: Comparison of tensile-torsion and compressive-torsion wood DMA. *Holzforschung* **2010**, *64*, 747–756. [CrossRef]
- 57. Harris, P.; Stone, B. Chemistry and Molecular Organization of Plant Cell Walls. In *Biomass Recalcitrance: Deconstructing the Plant Cell Wall for Bioenergy*, 1st ed.; Himme, M., Ed.; Blackwell: Chichester, UK, 2009; pp. 61–93.
- 58. Roland, J.; Reis, D.; Vian, B.; Roy, S. The helicoidal plant cell wall as a performing cellulose-based composite. *Mol. Biol. Cell.* **1989**, 67, 209–220. [CrossRef]
- 59. Hayot, C.; Forouzesh, E.; Goel, A.; Avramova, Z.; Turner, J. Viscoelastic properties of cell walls of single living plant cells determined by dynamic nanoindentation. *J. Exp. Bot.* **2012**, *63*, 2525–2540. [CrossRef]
- 60. Chen, L.; Liao, N.; Xing, L.; Han, L. Description of Wheat Straw Relaxation Behavior Based on a Fractional-Order Constitutive Model. *Agron. J.* **2013**, *105*, 134–142. [CrossRef]
- 61. Hu, J.J.; Lei, T.-Z.; Xu, G.-Y.; Shen, S.-Q.; Liu, J.-W. Experimental study of stress relaxation in the process of cold molding with straw. *BioResources* **2009**, *4*, 1158–1167. [CrossRef]
- 62. Liu, L.; Yu, W.; Jin, H. Modeling the stress-relaxation behavior of wool fibers. J. Appl. Polym. Sci. 2008, 110, 2078–2084. [CrossRef]
- 63. Tweedie, C.; Van Vliet, K. Contact creep compliance of viscoelastic materials via nanoindentation. *J. Mater. Res.* **2006**, 21, 1576–1589. [CrossRef]
- 64. Zhu, Y.; Fu, N.; Li, D.; Wang, L.; Chen, X. Physical and Viscoelastic Properties of Different Moisture Content Highland Barley Kernels. *Int. J. Food Eng.* **2017**, *13*, 20170186. [CrossRef]
- 65. Findely, W.N.; Lai, J.S.; Onaran, K. Nonlinear Creep at Constant Stress and Relaxation at Constant Strain. In *Creep and Relaxation of Nonlinear Viscoelastic Materials*; Findley, W.N., Lai, J.S., Onaran, K., Eds.; North-Holland: New York, NY, USA, 1976; pp. 176–219.

66. Ornaghi, H.; Almeida, J.; Monticeli, F.; Neves, R. Stress relaxation, creep, and recovery of carbon fiber non-crimp fabric composites. *Compos. Part C* **2020**, *3*, 100051. [CrossRef]

- 67. Siviour, C.; Jordan, J. High Strain Rate Mechanics of Polymers: A Review. J. Dyn. Behav. Mater. 2016, 2, 15–32. [CrossRef]
- 68. Roylance, D. *Engineering Viscoelasticity*; Massachusetts Institute of Technology: Cambridge, MA, USA, 2001. Available online: https://web.mit.edu/course/3/3.11/www/modules/visco.pdf (accessed on 10 October 2023).
- 69. Poletto, M.; Zattera, A.; Santana, R. Structural differences between wood species: Evidence from chemical composition, FTIR spectroscopy, and thermogravimetric analysis. *J. Appl. Polym. Sci.* **2012**, *126*, E337–E344. [CrossRef]
- 70. Acquah, G.; Via, B.; Fasina, O.; Eckhardt, L. Rapid Quantitative Analysis of Forest Biomass Using Fourier Transform Infrared Spectroscopy and Partial Least Squares Regression. *J. Anal. Methods Chem. J.* **2016**, 2016, 1839598. [CrossRef] [PubMed]
- 71. Faix, O. Classification of Lignins from Different Botanical Origins by FT-IR Spectroscopy. Holzforschung 1991, 45, 21–28. [CrossRef]
- 72. Isogai, A.; Usuda, M. Crystallinity Indexes of Cellulosic Materials. Sen'i Gakkaishi 1990, 46, 324–329. [CrossRef]
- 73. Segal, L.; Creely, J.J.; Martin, A.E.; Conrad, C.M. An empirical method for estimating the degree of crystallinity of native cellulose using the X-ray diffractometer. *Text. Res. J.* **1959**, *29*, 786–794. [CrossRef]
- 74. Park, S.; Baker, J.; Himmel, M.; Parilla, P.; Johnson, D. Cellulose crystallinity index: Measurement techniques and their impact on interpreting cellulase performance. *Biotechnol. Biofuels* **2010**, *3*, 10. [CrossRef]
- 75. Zhao, C.; Shao, Q.; Ma, Z.; Li, B.; Zhao, X. Physical and chemical characterizations of corn stalk resulting from hydrogen peroxide presoaking prior to ammonia fiber expansion pretreatment. *Ind. Crops Prod.* **2016**, *83*, 86–93. [CrossRef]
- 76. Vandenbrink, J.; Hilten, R.; Das, K.; Paterson, A.; Feltus, F. Analysis of crystallinity index and hydrolysis rates in the bioenergy crop *Sorghum bicolor. Bioenergy Res.* **2012**, *5*, 387–397. [CrossRef]
- 77. Reddy, N.; Yang, Y. Structure and properties of natural cellulose fibers obtained from sorghum leaves and stems. *J. Agric. Food Chem.* **2007**, *55*, 5569–5574. [CrossRef]
- 78. French, A.; Santiago Cintrón, M. Cellulose polymorphy, crystallite size, and the Segal Crystallinity Index. *Cellulose* **2013**, 20, 583–588. [CrossRef]
- 79. Parameswaran, N.; Liese, W. On the fine structure of bamboo fibres. Wood Sci. Technol. 1976, 10, 231–246. [CrossRef]
- 80. de Souza, M.; Lima, T.; Soares, D. Application of X-ray diffraction to assess the microfibril angle of green and dry Eucalyptus grandis wood. *Trees* **2022**, *36*, 191–197. [CrossRef]
- 81. Dungani, R.; Karina, M.; Subyakto, S.A.; Hermawan, D.; Hadiyane, A. Agricultural waste fibers towards sustainability and advanced utilization: A review. *Asian J. Plant Sci.* **2016**, *15*, 42–55. [CrossRef]
- 82. Venkateshwaran, N.; Elayaperumal, A.; Sathiya, G. Prediction of tensile properties of hybrid-natural fiber composites. *Compos. Part B Eng.* **2012**, *43*, 793–796. [CrossRef]
- 83. Driemeier, C.; Santos, D.; Buckeridge, S. Cellulose crystals in fibrovascular bundles of sugarcane culms: Orientation, size, distortion, and variability. *Cellulose* **2012**, *19*, 1507–1515. [CrossRef]
- 84. Tabet, T.; Aziz, F. Cellulose Microfibril Angle in Wood and Its Dynamic Mechanical Significance. In *Cellulose—Fundamental Aspects*; De Ven, T., Godbout, L., Eds.; IntechOpen: London, UK, 2013; pp. 113–142. [CrossRef]
- 85. Barnett, J.; Bonham, V. Cellulose microfibril angle in the cell wall of wood fibres. *Biol. Rev. Camb. Philos. Soc.* **2004**, *79*, 461–472. [CrossRef]
- 86. Kang, X.; Kirui, A.; Dickwella, C.; Mentink-Vigier, F.; Cosgrove, J.; Wang, T. Lignin-polysaccharide interactions in plant secondary cell walls revealed by solid-state NMR. *Nat. Commun.* **2019**, *10*, 347. [CrossRef]
- 87. Stubbs, C.; Larson, R.; Cook, D. Maize stalk stiffness and strength are primarily determined by morphological factors. *Sci. Rep.* **2022**, *12*, 720. [CrossRef] [PubMed]
- 88. Gibson, J. The hierarchical structure and mechanics of plant materials. J. R. Soc. Interface 2012, 9, 2749–2766. [CrossRef] [PubMed]
- 89. Rosado, M.; Bausch, F.; Rencoret, J.; Marques, G.; Gutiérrez, A.; Rosenau, T.; Potthast, A.; del Río, J. Differences in the content, composition and structure of the lignins from rind and pith of papyrus (*Cyperus papyrus* L.) culms. *Ind. Crops Prod.* **2021**, 174, 114226. [CrossRef]
- 90. Sequeiros, A.; Labidi, J. Characterization and determination of the S/G ratio via Py-GC/MS of agricultural and industrial residues. *Ind. Crops Prod.* **2017**, *97*, 469–476. [CrossRef]
- 91. Torri, C.; Adamiano, A.; Fabbri, D.; Lindfors, C.; Monti, A.; Oasmaa, A. Comparative analysis of pyrolysate from herbaceous and woody energy crops by Py-GC with atomic emission and mass spectrometric detection. *J. Anal. Appl. Pyrolysis* **2010**, *88*, 175–180. [CrossRef]
- 92. Liu, Q.; Luo, L.; Zheng, L. Lignins: Biosynthesis and Biological Functions in Plants. Int. J. Mol. Sci. 2018, 19, 335. [CrossRef]
- 93. Mengistie, E.; Alayat, A.; Sotoudehnia, F.; Bokros, N.; DeBolt, S.; McDonald, A.G. Evaluation of Cell Wall Chemistry of della and Its Mutant Sweet Sorghum Stalks. *J. Agric. Food Chem.* **2022**, *70*, 1689–1703. [CrossRef]
- 94. Li, X.; Chen, W.; Zhao, Y.; Xiang, Y.; Jiang, H.; Zhu, S.; Cheng, B. Downregulation of caffeoyl-CoA O-methyltransferase (CCoAOMT) by RNA interference leads to reduced lignin production in maize straw. *Genet. Mol. Biol.* **2013**, *36*, 540–546. [CrossRef]
- 95. Achyuthan, K.; Achyuthan, A.; Adams, P.; Dirk, S.; Harper, J.; Simmons, B.; Singh, A. Supramolecular Self-Assembled Chaos: Polyphenolic Lignin's Barrier to Cost-Effective Lignocellulosic Biofuels. *Molecules* **2010**, *15*, 8641–8688. [CrossRef]
- 96. Verma, S.; Dwivedi, U. Lignin genetic engineering for improvement of wood quality: Applications in paper and textile industries, fodder and bioenergy production. *S. Afr. J. Bot.* **2014**, *91*, 107–125. [CrossRef]

97. Ziebell, A.; Gracom, K.; Katahira, R.; Chen, F.; Pu, Y.; Ragauskas, A.; Dixon, R.; Davis, M. Increase in 4-coumaryl alcohol units during lignification in alfalfa (*Medicago sativa*) alters the extractability and molecular weight of lignin. *J. Biol. Chem.* **2010**, 285, 38961–38968. [CrossRef] [PubMed]

- 98. Cesarino, I.; Araújo, P.; Domingues, P.; Mazzafera, P. An overview of lignin metabolism and its effect on biomass recalcitrance. *Braz. J. Bot.* **2012**, *35*, 303–311. [CrossRef]
- 99. Ferrer, J.; Austin, M.; Stewart, C.; Noel, J. Structure and function of enzymes involved in the biosynthesis of phenylpropanoids. *Plant Physiol. Biochem.* **2008**, *46*, 356–370. [CrossRef] [PubMed]
- 100. Hu, D.; Liu, X.; She, H.; Gao, Z.; Ruan, R.; Wu, D.; Yi, Z. The lignin synthesis related genes and lodging resistance of *Fagopyrum* esculentum. Biol. Plant. **2016**, 61, 138–146. [CrossRef]
- 101. Wei, L.; Jian, H.; Lu, K.; Yin, N.; Wang, J.; Duan, X.; Li, W.; Liu, L.; Xu, X.; Wang, R.; et al. Genetic and transcriptomic analyses of lignin- and lodging-related traits in *Brassica napus*. *Theor. Appl. Genet.* **2017**, *130*, 1961–1973. [CrossRef] [PubMed]
- 102. Li, F.; Zhang, M.; Guo, K.; Hu, Z.; Zhang, R.; Feng, Y.; Yi, X.; Zou, W.; Wang, L.; Wu, C.; et al. High-level hemicellulosic arabinose predominately affects lignocellulose crystallinity for genetically enhancing both plant lodging resistance and biomass enzymatic digestibility in rice mutants. *Plant Biotechnol. J.* 2015, 13, 514–525. [CrossRef]
- 103. Luo, Y.; Ni, J.; Pang, D.; Jin, M.; Chen, J.; Kong, X.; Li, W.; Chang, Y.; Li, Y.; Wang, Z. Regulation of lignin composition by nitrogen rate and density and its relationship with stem mechanical strength of wheat. *Field Crops Res.* **2019**, 241, 107572. [CrossRef]
- 104. Rencoret, J.; Gutiérrez, A.; Nieto, L.; Jiménez-Barbero, J.; Faulds, C.; Kim, H.; Ralph, J.; Martínez, Á.; del Río, J. Lignin Composition and Structure in Young versus Adult *Eucalyptus globulus* Plants. *Plant Physiol.* **2011**, *155*, 667–682. [CrossRef]
- 105. Li, M.; Pu, Y.; Ragauskas, J. Current understanding of the correlation of lignin structure with biomass recalcitrance. *Front. Chem.* **2016**, *4*, 45. [CrossRef]
- 106. Manga-Robles, A.; Santiago, R.; Malvar, R.; Moreno-González, V.; Fornalé, S.; López, I.; Centeno, M.; Acebes, J.; Álvarez, J.; Caparros-Ruiz, D.; et al. Elucidating compositional factors of maize cell walls contributing to stalk strength and lodging resistance. *Plant Sci.* 2021, 307, 110882. [CrossRef] [PubMed]
- 107. Del Río, C.; Rencoret, J.; Prinsen, P.; Martínez, T.; Ralph, J.; Gutiérrez, A. Structural characterization of wheat straw lignin as revealed by analytical pyrolysis, 2D-NMR, and reductive cleavage methods. *J. Agric. Food Chem.* **2012**, *60*, 5922–5935. [CrossRef] [PubMed]
- 108. Huang, J.; Liu, W.; Zhou, F.; Peng, Y. Effect of multiscale structural parameters on the mechanical properties of rice stems. *J. Mech. Behav. Biomed. Mater.* **2018**, *82*, 239–247. [CrossRef] [PubMed]
- 109. Rivera-Burgos, L.; Volenec, J.; Ejeta, G. Biomass and Bioenergy Potential of Brown Midrib Sweet Sorghum Germplasm. *Front. Plant Sci.* **2019**, *10*, 1142. [CrossRef]
- 110. Genet, M.; Stokes, A.; Salin, F.; Mickovski, S.; Fourcaud, T.; Dumail, J.; Van Beek, R. The Influence of Cellulose Content on Tensile Strength in Tree Roots. *Plant Soil.* **2005**, *278*, 1–9. [CrossRef]
- 111. Sánchez-Echeverri, L.; Aita, G.; Robert, D.; Rodriguez, M. Correlation between chemical compounds and mechanical response in culms of two different ages of *Guadua angustifolia* Kunth. *Madera Bosques* **2014**, 20, 87–94. [CrossRef]
- 112. Chen, G.; Shi, Y.; Yin, P.; Wang, L.; Shi, H.; Peng, L.; Ni, L.; Cai, T. Relationship between Lignin Metabolism and Lodging Resistance in Wheat. *Acta Agron. Sin.* **2011**, *37*, 1616–1622. [CrossRef]
- 113. Wu, L.; Zhang, W.; Ding, Y.; Zhang, J.; Cambula, E.; Weng, F.; Liu, Z.; Ding, C.; Tang, S.; Chen, L.; et al. Shading contributes to the reduction of stem mechanical strength by decreasing cell wall synthesis in japonica rice (*Oryza sativa* L.). *Front. Plant Sci.* **2017**, *8*, 881. [CrossRef]
- 114. Peng, D.; Chen, X.; Yin, Y.; Lu, K.; Yang, W.; Tang, Y.; Wang, Z. Lodging resistance of winter wheat (*Triticum aestivum* L.): Lignin accumulation and its related enzymes activities due to the application of paclobutrazol or gibberellin acid. *Field Crops Res.* **2014**, 157, 1–7. [CrossRef]
- 115. Turner, S.; Somerville, C. Collapsed xylem phenotype of Arabidopsis identifies mutants deficient in cellulose deposition in the secondary cell wall. *Plant Cell* **1997**, *9*, 689–701. [CrossRef]
- 116. Hondroyianni, P.D.; Gagianas, A.; Tsatsarelis, K. Corn stalk traits related to lodging resistance in two soils of differing salinity. *Maydica* **2000**, *45*, 125–133.
- 117. Kaack, K.; Schwarz, K.; Brander, P. Variation in morphology, anatomy and chemistry of stems of Miscanthus genotypes differing in mechanical properties. *Ind. Crops Prod.* **2003**, *17*, 131–142. [CrossRef]
- 118. Okuno, A.; Hirano, K.; Asano, K.; Takase, W.; Masuda, R.; Morinaka, Y.; Ueguchi-Tanaka, M.; Kitano, H.; Matsuoka, M. New Approach to Increasing Rice Lodging Resistance and Biomass Yield Through the Use of High Gibberellin Producing Varieties. *PLoS ONE* **2014**, *9*, e86870. [CrossRef] [PubMed]
- 119. Wei, F. Effects of Nitrogenous Fertilizer Application Model on Culm Lodging Resistance in Winter Wheat. *Acta Agron. Sin.* **2008**, 34, 1080–1085. [CrossRef]
- 120. Voelker, S.; Lachenbruch, B.; Meinzer, F.; Strauss, S. Reduced wood stiffness and strength, and altered stem form, in young antisense 4CL transgenic poplars with reduced lignin contents. *New Phytol.* **2011**, *189*, 1096–1109. [CrossRef] [PubMed]
- 121. Zhang, Y.; Wang, Y.; Ye, D.; Wang, W.; Qiu, X.; Duan, L.; Li, Z.; Zhang, M. Ethephon Improved Stalk Strength of Maize (*Zea Mays* L.) Mainly through Altering Internode Morphological Traits to Modulate Mechanical Properties under Field Conditions. *Agronomy* 2019, 9, 186. [CrossRef]

122. Liu, S.; Huang, Y.; Xu, H.; Zhao, M.; Xu, Q.; Li, F. Genetic enhancement of lodging resistance in rice due to the key cell wall polymer lignin, which affects stem characteristics. *Breed Sci.* **2018**, *68*, 508–515. [CrossRef]

- 123. Petti, C.; Harman-Ware, A.E.; Tateno, M.; Kushwaha, R.; Shearer, A.; Downie, A.B.; Crocker, M.; DeBolt, S. Sorghum mutant RGdisplays antithetic leaf shoot lignin accumulation resulting in improved stem saccharification properties. *Biotechnol. Biofuels* **2013**, *6*, 146. [CrossRef]
- 124. Xu, Q.; Engquist, B. A mathematical model for fitting and predicting relaxation modulus and simulating viscoelastic responses. *Proc. R. Soc.* **2018**, *474*, 2213. [CrossRef]
- 125. Simsiriwong, J.; Sullivan, R.; Hilton, H. Viscoelastic creep compliance using prony series and spectrum function approach. In *Challenges in Mechanics of Time-Dependent Materials and Processes in Conventional and Multifunctional Materials*; Antoun, B., Qi, H., Hall, R., Tandon, G., Lu, H., Lu, C., Eds.; Springer: New York, NY, USA, 2013; Volume 2, pp. 149–160.
- 126. Schöning, J.G. Absorptiometric determination of acid-soluble lignin in semichemical bisulfite pulps and in some woods and plants. *Sven. Papperstidning-Nord. Cellul.* **1965**, *68*, 607–613.
- 127. Yamamoto, H.; Okuyama, T.; Yoshida, M. Method of determining the mean microfibril angle of wood over a wide range by the improved Cave's method. *J. Jpn. Wood Res. Soc.* **1993**, *39*, 375–381.
- 128. Cave, D. Theory of X-ray measurement of microfibril angle in wood. Wood Sci. Technol. 1997, 31, 143–152. [CrossRef]
- 129. Rekha, B.; Nagarajaganesh, B. X-ray Diffraction: An Efficient Method to Determine Microfibrillar Angle of Dry and Matured Cellulosic Fibers. *J. Nat. Fibers* **2020**, *19*, 3689–3696. [CrossRef]
- 130. Faix, O.; Meier, D.; Fortmann, I. Thermal degradation products of wood. Holz Als Roh-Und Werkstoff 1990, 48, 351-354. [CrossRef]
- 131. Meier, D.; Faix, O. Pyrolysis-Gas Chromatography-Mass Spectrometry. In *Methods in Lignin Chemistry*; Lin, S., Dence, C., Eds.; Springer Series in Wood Science; Springer: Berlin/Heidelberg, Germany, 1992; pp. 177–199.
- 132. Lu, F.; Ralph, J. Derivatization Followed by Reductive Cleavage (DFRC Method), a New Method for Lignin Analysis: Protocol for Analysis of DFRC Monomers. *J. Agric. Food Chem.* **1997**, *45*, 2590–2592. [CrossRef]
- 133. Lu, F.; Ralph, J. The DFRC Method for Lignin Analysis. 2. Monomers from Isolated Lignins. *J. Agric. Food Chem.* **1998**, 46, 547–552. [CrossRef] [PubMed]

**Disclaimer/Publisher's Note:** The statements, opinions and data contained in all publications are solely those of the individual author(s) and contributor(s) and not of MDPI and/or the editor(s). MDPI and/or the editor(s) disclaim responsibility for any injury to people or property resulting from any ideas, methods, instructions or products referred to in the content.